



1 **Organic peroxy radical chemistry in oxidation flow reactors and environmental chambers**
2 **and their atmospheric relevance**

3 Zhe Peng¹, Julia Lee-Taylor^{1,2}, John J. Orlando², Geoffrey S. Tyndall² and Jose L. Jimenez¹

4 ¹ Cooperative Institute for Research in Environmental Sciences and Department of Chemistry,
5 University of Colorado, Boulder, Colorado 80309, USA

6 ² Atmospheric Chemistry Observation and Modeling Laboratory, National Center for Atmospheric
7 Research, Boulder, Colorado 80307, USA

8
9 Correspondence: Zhe Peng (zhe.peng@colorado.edu) and Jose L. Jimenez
10 (jose.jimenez@colorado.edu)
11

12 **Abstract.** Oxidation flow reactors (OFR) are a promising complement to environmental chambers for
13 investigating atmospheric oxidation processes and secondary aerosol formation. However, questions
14 have been raised about how representative the chemistry within OFRs is of that in the troposphere. We
15 investigate the fates of organic peroxy radicals (RO₂), which play a central role in atmospheric organic
16 chemistry, in OFRs and environmental chambers by chemical kinetic modeling, and compare to a variety
17 of ambient conditions to help define a range of atmospherically relevant OFR operating conditions. For
18 most types of RO₂, their bimolecular fates in OFRs are mainly RO₂+HO₂ and RO₂+NO, similar to chambers
19 and atmospheric studies. For substituted primary RO₂ and acyl RO₂, RO₂+RO₂ can make a significant
20 contribution to the fate of RO₂ in OFRs, chambers and the atmosphere, but RO₂+RO₂ in OFRs is in general
21 somewhat less important than in the atmosphere. At high NO, RO₂+NO dominates RO₂ fate in OFRs, as
22 in the atmosphere. At high UV lamp setting in OFRs, RO₂+OH can be a major RO₂ fate and RO₂
23 isomerization can be negligible for common multifunctional RO₂, both of which deviate from common
24 atmospheric conditions. In the OFR254 operation mode (where OH is generated only from photolysis
25 of added O₃), we cannot identify any conditions that can simultaneously avoid significant organic
26 photolysis at 254 nm and lead to RO₂ lifetimes long enough (~10 s) to allow atmospherically relevant
27 RO₂ isomerization. In the OFR185 mode (where OH is generated from reactions initiated by 185 nm
28 photons), high relative humidity, low UV intensity and low precursor concentrations are recommended
29 for atmospherically relevant gas-phase chemistry of both stable species and RO₂. These conditions
30 ensure minor or negligible RO₂+OH and a relative importance of RO₂ isomerization in RO₂ fate in OFRs
31 within ~x2 of that in the atmosphere. Under these conditions, the photochemical age within OFR185
32 systems can reach a few equivalent days at most, encompassing the typical ages for maximum
33 secondary organic aerosol (SOA) production. A small increase in OFR temperature may allow the relative
34 importance of RO₂ isomerization to approach the ambient values. To study heterogeneous oxidation of
35 SOA formed under atmospherically-relevant OFR conditions, a different UV source with higher intensity
36 is needed after the SOA formation stage, which can be done with another reactor in series. Finally, we
37 recommend evaluating the atmospheric relevance of RO₂ chemistry by always reporting measured
38 and/or estimated OH, HO₂, NO, NO₂ and OH reactivity (or at least precursor composition and
39 concentration) in all chamber and flow reactor experiments. An easy-to-use RO₂ fate estimator program
40 is included with this paper to facilitate investigation of this topic in future studies.



41 1 Introduction

42 Laboratory reactors are needed to isolate and study atmospheric chemical systems. Environmental
43 chambers have been a major atmospheric chemistry research tool for decades (Cocker et al., 2001;
44 Carter et al., 2005; Presto et al., 2005; Wang et al., 2011; Platt et al., 2013). Over the last few years,
45 oxidation flow reactors (OFRs) (Kang et al., 2007) have emerged as a promising complement to
46 chambers, and are being used to investigate atmospheric oxidation processes, particularly volatile
47 organic compound (VOC) oxidation and secondary organic aerosol (SOA) formation and aging (Kang et
48 al., 2011; Lambe et al., 2015; Hu et al., 2016; Palm et al., 2016). These processes have air quality (Levy
49 II, 1971), human health (Nel, 2005) and climate impacts (Stocker et al., 2014).

50 The most important advantage of OFRs is their ability to achieve relatively high photochemical
51 ages (on the order of equivalent hours or days (assuming an average ambient OH concentration of
52 1.5×10^6 molecules cm^{-3} ; Mao et al., 2009) in minutes instead of hours in chambers (Lambe et al., 2011).
53 Rapid aging is usually achieved by highly active HO_x radical chemistry initiated by low-pressure Hg lamp
54 emissions (185 and 254 nm) (Li et al., 2015; Peng et al., 2015). This allows shorter residence times in
55 OFRs thus reducing gas and particle losses to walls, which can be very important in Teflon chambers
56 (Cocker et al., 2001; Matsunaga and Ziemann, 2010; Zhang et al., 2014; Krechmer et al., 2016). In
57 addition, lower costs and small size (volumes of the order of 10 L) of OFRs allow better portability. These,
58 together with the ability to rapidly achieve high photochemical ages, are advantageous for field
59 applications.

60 These advantages of OFRs have led a number of atmospheric chemistry research groups (Lambe
61 and Jimenez, 2018) to deploy them in field (Hu et al., 2016; Ortega et al., 2016; Palm et al., 2016, 2017),
62 source (Ortega et al., 2013; Tkacik et al., 2014; Karjalainen et al., 2016; Link et al., 2016) and laboratory
63 studies (Kang et al., 2011; Lambe et al., 2013; Richards-Henderson et al., 2016; Lim et al., 2017).
64 However, the atmospheric relevance of VOC oxidation and SOA formation simulated in OFRs has
65 repeatedly been called into question, because the UV wavelengths most commonly used to initiate OFR
66 chemistry do not exist in the troposphere, and because OH levels in OFRs (10^8 – 10^{10} molecules cm^{-3}) can
67 be much higher than tropospheric levels (10^6 – 10^7 molecules cm^{-3} ; Mao et al., 2009; Stone et al., 2012)
68 To clarify this issue, a series of chemical kinetic modeling studies have been performed: Li et al. (2015)
69 and Peng et al. (2015) established a radical chemistry and oxidation model whose predictions compare
70 well against laboratory experiments and found that OH can be substantially suppressed by external OH
71 reactants (e.g. SO_2 , NO_x and VOCs externally introduced into the reactor); Peng et al. (2016) identified
72 low water mixing ratio (H_2O) and/or high external OH reactivity (OHR_{ext} , i.e. first-order OH loss rate
73 constant contributed by external OH reactants) as conditions that can cause significant non-
74 tropospheric VOC reactions (e.g. through photolysis at 185 and/or 254 nm); Peng and Jimenez (2017)
75 studied NO_x chemistry in OFRs and showed that high- NO conditions, where organic peroxy radicals react
76 more rapidly with NO than with HO_2 , can only be realized by simple NO injection in a very narrow range
77 of physical conditions, whose application to investigating intermediate- and high- NO environments (e.g.
78 urban area) is limited; Peng et al. (2018) thus evaluated a few new techniques to maintain high- NO



79 conditions in OFRs and found injection of percent-level N_2O effective to achieve this goal.

80 While HO_x and NO_y chemistries have been extensively characterized in OFRs so far, organic peroxy
81 radical (RO_2) chemistry has yet to be considered in detail, as previous studies have only considered the
82 balance between RO_2+NO vs RO_2+HO_2 . There has been some speculation that due to high OH
83 concentrations in OFRs, RO_2 concentration and lifetime might be significantly different from ambient
84 values, leading to dominance of RO_2 self/cross reactions and elimination of RO_2 isomerization pathways
85 (Crounse et al., 2013; Praske et al., 2018). Given the central role RO_2 plays in atmospheric chemistry
86 (Orlando and Tyndall, 2012; Ziemann and Atkinson, 2012) and the rapidly increasing use of OFRs, RO_2
87 chemistry in OFRs needs to be studied in detail to characterize the similarities and differences between
88 their reactions conditions and those in the ambient atmosphere and traditional atmospheric reaction
89 chambers.

90 In this paper, we address this need via modeling. All major known fates of RO_2 in OFRs will be
91 investigated and compared with those in typical chamber cases and in the atmosphere. This comparison
92 will provide insights into the atmospheric relevance of RO_2 chemistry in atmospheric simulation reactors
93 and allow the selection of experimental conditions with atmospherically relevant RO_2 chemistry in
94 experimental planning.

95 **2 Methods**

96 Due to a variety of loss pathways of RO_2 and a myriad of RO_2 types, RO_2 chemistry is of enormous
97 complexity. We detail the RO_2 production and loss pathways of interest in this study, the approximations
98 used to simplify this complex problem, and steps to investigate it methodically. We briefly introduce the
99 base OFR design and the model, which are described in detail elsewhere (Kang et al., 2007; Peng et al.,
100 2015, 2018).

101 **2.1 Potential Aerosol Mass oxidation flow reactor (PAM OFR)**

102 The concept of the base OFR design simulated in this study, the Potential Aerosol Mass (PAM)
103 reactor, was first introduced by Kang et al. (2007) The geometry of the most popular PAM OFR is a
104 cylinder of ~ 13 L volume. The PAM reactor we simulate is equipped with low-pressure Hg lamps (model
105 no. 82-9304-03, BHK Inc.) emitting UV light at 185 and 254 nm. When both 185 and 254 nm photons
106 are used to generate OH (termed “OFR185”), water vapor photolysis at 185 nm produces OH and HO_2 .
107 Recombination of O_2 and $\text{O}(^3\text{P})$, formed by O_2 photolysis at 185 nm, generates O_3 . $\text{O}(^1\text{D})$, formed through
108 O_3 photolysis at 254 nm, reacts with water vapor and produces additional OH. 185 nm photons can be
109 filtered by installing quartz sleeves around the lamps. This converts the reactor into “OFR254” mode,
110 where photolysis of O_3 , which must be initially injected, is the only OH production route. The notation
111 “OFR254-X” is used to specify the initial amount of injected O_3 (X ppm) in OFR254. Lambe et al. (2017)
112 and Peng et al. (2018) have shown that initial injection of N_2O is able to maintain up to tens of ppb NO
113 in both OFR185 and OFR254. These modes are denoted “OFR185-i N_2O ” and “OFR254-X-i N_2O ”, or more
114 generally “OFR-i N_2O ”. In OFR254-i N_2O , $\text{O}(^1\text{D})$ generated from O_3 photolysis reacts with N_2O to generate
115 NO, while in OFR185-i N_2O , $\text{O}(^1\text{D})$ is mainly supplied by N_2O photolysis at 185 nm (Peng et al., 2018).

116 **2.2 RO_2 production and loss pathways**



117 A single generic RO₂ is adopted for modeling purposes, to avoid the huge number of RO₂ types
118 that would complicate effective modeling and analysis. In OH-initiated VOC oxidation, RO₂ is primarily
119 produced via VOC+OH → R (+H₂O) followed by R+O₂ → RO₂, where R is hydrocarbonyl or oxygenated
120 hydrocarbonyl radical. Since the second step is extremely fast in air (Atkinson and Arey, 2003), the first
121 step controls the RO₂ production rate, which depends on OH concentration and OHR_{ext} due to VOCs
122 (OHR_{VOC}, see Appendix A for details). OHR_{VOC} also includes the contribution from oxidation
123 intermediates of primary VOCs (e.g. methyl vinyl ketone and pinonic acid). When the information about
124 oxidation intermediates is insufficient to calculate OHR_{VOC}, OHR due to primary VOCs is used instead as
125 an approximant.

126 Table 1 lists all known RO₂ loss pathways. Among those, RO₂ photolysis, RO₂+NO₃ and RO₂+O₃
127 are not included in this study, since they are minor or negligible in OH-dominated atmospheres,
128 chambers and OFRs for the following reasons.

- 129 - The first-order RO₂ photolysis rate constant is of the order of 10⁻² s⁻¹ at the highest lamp setting in
130 OFRs (Kalafut-Pettibone et al., 2013) and of the order of 10⁻⁵ s⁻¹ in the troposphere under the
131 assumption of unity quantum yield (Klems et al., 2015), while RO₂ reacts with HO₂ at >1 s⁻¹ at the
132 highest lamp setting in OFRs and at ~2×10⁻³ s⁻¹ in the troposphere. Note that in this study we assume
133 an average ambient HO₂ concentration of 1.5×10⁸ molecules cm⁻³ (Mao et al., 2009; Stone et al.,
134 2012) and RO₂+HO₂ rate constant of 1.5×10⁻¹¹ cm³ molecule⁻¹ s⁻¹ (Orlando and Tyndall, 2012).
- 135 - When daytime photochemistry is active, NO₃ is negligible in the atmosphere. In OFR-iN₂O modes,
136 RO₂+NO₃ is negligible unless at very low H₂O and high UV intensity (abbr. UV hereafter), which
137 result in high O₃ to oxidize NO₂ to NO₃ and keep HO₂ minimized. However, very low H₂O causes
138 serious non-tropospheric organic photolysis (Peng et al., 2016) and thus these conditions are of no
139 experimental interest.
- 140 - In the atmosphere RO₂+O₃ is thought to play some role only at night (Orlando and Tyndall, 2012).
141 Similar conditions may exist in some OFR254 cases, if a very large amount of O₃ is injected and H₂O
142 and UV are kept very low to limit HO_x production. These conditions are obviously not OH-
143 dominated and not further investigated in this study.

144 Of the RO₂ fates considered in this study, RO₂+HO₂ and RO₂+NO and RO₂+RO₂ have long been
145 known to play a role in the atmosphere (Orlando and Tyndall, 2012). Despite some small dependencies
146 on the type of RO₂, recommended general rate constants are available for RO₂+HO₂ and RO₂+NO
147 (Ziemann and Atkinson, 2012; Table 1). We use these recommended values for generic RO₂ in this study.
148 However, RO₂ self-/cross-reaction rate constants are highly dependent on the specific RO₂ types and can
149 vary over a very large range (10⁻¹⁷–10⁻¹⁰ cm³ molecule⁻¹ s⁻¹). Unsubstituted primary, secondary and
150 tertiary RO₂ self-react at ~10⁻¹³, ~10⁻¹⁵ and ~10⁻¹⁷ cm³ molecule⁻¹ s⁻¹, respectively (Ziemann and Atkinson,
151 2012). Rate constants of cross-reactions between these RO₂ types also span this range (Orlando and
152 Tyndall, 2012). Substituted RO₂s have higher self-/cross-reaction rate constants (Orlando and Tyndall,
153 2012). RO₂+RO₂ of highly substituted primary RO₂ can be as high as ~10⁻¹¹ cm³ molecule⁻¹ s⁻¹ (Orlando
154 and Tyndall, 2012). Very recently, a few highly oxidized 1,3,5-trimethylbenzene-derived RO₂s were



155 reported to self-/cross-react at $\sim 10^{-10}$ cm³ molecule⁻¹ s⁻¹ (Berndt et al., 2018). In the present work, we
156 make a simplification to adapt to the generic RO₂ treatment by assuming a single self-/cross-reaction
157 rate constant for generic RO₂ in each case. Three levels of RO₂+RO₂ rate constants, i.e. 1×10^{-13} , 1×10^{-11} ,
158 and 1×10^{-10} cm³ molecule⁻¹ s⁻¹, are studied in this paper. The first level is referred to as “medium RO₂+RO₂”
159 as many other RO₂ can have self-/cross-reaction rate constants as low as 10^{-17} cm³ molecule⁻¹ s⁻¹; the
160 second level is defined as “fast RO₂+RO₂”; the last level is called “very fast RO₂+RO₂.” No RO₂+RO₂ rate
161 constant lower than the medium level is investigated in the current work, although there are still a large
162 variety of RO₂ whose self-/cross reactions are at lower rate constants, since at the medium level,
163 RO₂+RO₂ is already negligible in all the environments studied in this work, i.e. OFRs, chambers and the
164 atmosphere (see Section 3.1.1). Since there are only a few very specific examples for very fast RO₂+RO₂
165 reported to date, we will not systematically explore this category but compare very fast RO₂+RO₂ as a
166 sensitivity case with the other two types of RO₂+RO₂ reactions.

167 Acyl RO₂ is considered as a separate RO₂ type (neither medium nor fast RO₂+RO₂) in this study
168 since its reaction with NO₂ can be a major sink of RO₂ in OFR (Peng and Jimenez, 2017). Thermal
169 decomposition lifetimes of the product of RO₂+NO₂, i.e. acylperoxy nitrates, can be hours at laboratory
170 temperatures (Orlando and Tyndall, 2012; also taken into account in the current work, see Table 1),
171 while OFR residence times are typically minutes. Besides, acyl RO₂ react with many RO₂ at $\sim 10^{-11}$ cm³
172 molecule⁻¹ s⁻¹ (Orlando and Tyndall, 2012), similar to that of fast RO₂+RO₂. We thus assume acyl RO₂
173 self-/cross-reaction rate constant to be also 1×10^{-11} cm³ molecule⁻¹ s⁻¹ to facilitate the comparison with
174 fast RO₂+RO₂ results.

175 In OFRs operated at room temperature, acylperoxy nitrates barely decompose, while peroxy
176 nitrates of non-acyl RO₂ do decompose on a timescale of 0.1 s (Table 1). As a consequence, the
177 production and decomposition of peroxy nitrates of non-acyl RO₂ reach a steady state in OFRs, which
178 can be greatly shifted toward the peroxy nitrate side in cases with very high NO₂ (Peng and Jimenez,
179 2017; Peng et al., 2018).

180 RO₂+OH (Fittschen et al., 2014) and RO₂ isomerization (Crouse et al., 2013) have recently been
181 identified as possible significant RO₂ fates in the atmosphere. Reactions of the former type, according
182 to several recent experimental and theoretical studies (Bossolasco et al., 2014; Assaf et al., 2016, 2017b,
183 2017a; Müller et al., 2016; Yan et al., 2016), have similar rate constants ($\sim 1 \times 10^{-10}$ cm³ molecule⁻¹ s⁻¹)
184 regardless of RO₂ type. Therefore, the reaction rate constant of generic RO₂ with OH is assigned as 1×10^{-10}
185 cm³ molecule⁻¹ s⁻¹. RO₂ isomerization reactivity is highly structure-dependent (Crouse et al., 2013;
186 Praske et al., 2018) and rate constant measurements are still scarce, preventing us from assigning a
187 generic RO₂ isomerization rate constant. However, for *generic* RO₂, isomerization is generally *not* a sink
188 but a conversion between two RO₂ (both encompassed by the generic one in this study), as RO₂
189 isomerization usually generates an oxygenated hydrocarbyl radical, which rapidly recombines with O₂
190 and forms another RO₂. Therefore, RO₂ isomerization is not explicitly taken into account in the modeling,
191 but is considered in the RO₂ fate analysis.

192 In summary, 6 pathways are included in the RO₂ fate analysis of this study. The need to explore



193 these 6 pathways for a high number of OFR, chamber, and atmospheric conditions makes presentation
194 of results challenging. For clarity, we present the results in two steps. In the first step, only well-known
195 RO₂ fates (reaction with NO₂, HO₂, NO and RO₂) will be included in the model. In the second step, the
196 results of the first step will be used to guide the modeling and analysis of a more comprehensive set of
197 significant RO₂ fates.

198 2.3 Model description

199 The model used in the present work is a standard chemical kinetic box model, implemented in the
200 KinSim 3.4 solver in Igor Pro 7 (WaveMetrics, Lake Oswego, Oregon, USA), and has been described in
201 detail elsewhere (Peng et al., 2015, 2018). Plug flow in the reactor with a residence time of 180 s is
202 assumed, since the effects of non-plug flow are major only in a narrow range of conditions of little
203 experimental interest and the implementation of laminar flow or measured residence time distribution
204 substantially increases computational cost (Peng et al., 2015; Peng and Jimenez, 2017). The reactions
205 of RO₂ discussed in Section 2.2 are added to the chemical mechanism. A generic slow-reacting VOC
206 (with the same OH rate constant as SO₂) is used as the external OH reactant. This slow rate also
207 represents the generation and consumption of latter-generation products that continue to react with
208 OH. The reason for this approximation has been discussed in detail in previous OFR modeling papers
209 (Peng and Jimenez, 2017; Peng et al., 2018). We exclude NO_y species, which are explicitly modeled, from
210 the calculation of OHR_{ext}; thus OHR_{ext} only includes non-NO_y OHR_{ext} hereafter. As OHR_{ext} is dominated
211 by OHR_{VOC} in most OFR experiments, we use OHR_{ext} to denote OHR_{VOC} in OFRs (while for ambient and
212 chamber cases OHR_{VOC} is still used to exclude the contribution of CO etc.). The model was estimated to
213 achieve an accuracy of a factor of 2–3 when compared to field OFR experiments; better agreement can
214 generally be obtained for laboratory OFR experiments (Li et al., 2015; Peng et al., 2015).

215 Another key parameter in the model is the HO_x recycling ratio (β), defined in this study as the
216 number of HO₂ molecule(s) produced per OH molecule destroyed by external OH reactants (Peng et al.,
217 2015). This ratio depends on the products of RO₂ loss pathways. The main product of RO₂+HO₂ is usually
218 ROOH (Table 1), yielding no recycled HO₂, while the main products of RO₂+NO are RO and NO₂, the
219 former of which can often undergo extremely fast H-abstraction by O₂ to form a carbonyl and HO₂. From
220 VOC oxidation simulations by the fully explicit model GECKO-A (Aumont et al., 2005), we estimate $\beta \sim 0.3$
221 in zero-NO OFRs. At the other extreme, where RO₂ is solely consumed by RO₂+NO, the product RO yields
222 HO₂ at a branching ratio close to 1, $\beta \sim 1$. For intermediate cases, we assume that β may be interpolated
223 as a linear function of $r(\text{RO}_2+\text{NO})/[r(\text{RO}_2+\text{NO})+r(\text{RO}_2+\text{HO}_2)]$, where $r(\text{RO}_2+\text{NO})$ and $r(\text{RO}_2+\text{HO}_2)$ are the
224 local reactive fluxes of RO₂+NO and RO₂+HO₂.

225 In the present work, we model OFR185, OFR254-70, and OFR254-7 (including their -iN₂O variants).
226 We specify the same temperature and atmospheric pressure (295 K and 835 mbar, typical values in
227 Boulder, Colorado, USA) as our previous OFR modeling studies (Li et al., 2015; Peng et al., 2015, 2016,
228 2018; Peng and Jimenez, 2017). The explored physical condition space follows that of our previous OFR-
229 iN₂O modeling work (Peng et al., 2018). The only differences are that in this study we also include cases
230 without any N₂O injected (OFR185 and OFR254 only) and exclude OHR_{ext}=0 conditions, which produce



231 no RO₂. In detail, the explored physical condition space covers: H₂O of 0.07–2.3% (relative humidity of
232 2–71% at 295 K); UV photon flux at 185 nm (abbr. F185) of 1.0x10¹¹–1.0x10¹⁴ photons cm⁻² s⁻¹
233 [corresponding photon flux at 254 nm (F254) of 4.2x10¹³–8.5x10¹⁵ photons cm⁻² s⁻¹]; OHR_{ext} of 1–1000
234 s⁻¹; N₂O mixing ratio (abbr. N₂O hereafter) of 0 and 0.02–20%. All model cases are logarithmically evenly
235 distributed except for N₂O=0 and F254. The latter is calculated based on the F185–F254 relationship for
236 the lamps simulated here (Li et al., 2015).

237 For the classification of conditions, the same criteria as in the OFR-iN₂O modeling study (Peng et
238 al., 2018) are adopted. In detail, high- and low-NO conditions are classified by $r(\text{RO}_2+\text{NO})/r(\text{RO}_2+\text{HO}_2)$.
239 In the current work, these reactive fluxes are explicitly tracked in the modeling instead of approximated
240 as in previous studies (Peng and Jimenez, 2017; Peng et al., 2018). The terms “good,” “risky” and “bad”
241 are used to describe OFR operating conditions in terms of non-tropospheric organic photolysis, and are
242 defined based on the ratios of F185 and F254 exposure (F185_{exp} and F254_{exp}, i.e. integrated photon
243 fluxes over residence time) to OH exposure (OH_{exp}), as presented previously (Peng and Jimenez, 2017;
244 Peng et al., 2018). Briefly, under a given condition non-tropospheric photolysis is of different relative
245 importance in the fate of each specific organic species: under good conditions, photolysis at 185 and/or
246 254 nm is unimportant for almost all VOCs; under bad conditions, non-tropospheric photolysis is
247 problematic for most VOC precursors, since significant photolysis of their oxidation intermediates at
248 185 and/or 254 nm is almost inevitable; and risky conditions can be problematic for some but not all
249 VOCs. Note that good/risky/bad conditions refer only to non-tropospheric organic photolysis and *not* to
250 whether RO₂ chemistry is atmospherically relevant. Table S1 summarizes our condition classification
251 criteria.

252 3 Results and discussion

253 In this section, the results are presented in two parts, i.e. first for the simulations with well-known
254 pathways only, and secondly with all significant pathways, as proposed in Section 2.2. Then based on
255 the results and their comparison with the atmosphere and chamber experiments, we propose
256 guidelines for OFR operation to ensure atmospherically relevant RO₂ chemistry, as well as other
257 chemistries already discussed in the previous studies (Peng et al., 2016, 2018), in OFRs.

258 3.1 Simulations with well-known pathways (RO₂+HO₂, RO₂+RO₂, RO₂+NO and RO₂+NO₂)

259 Due to significantly different reactivities of non-acyl and acyl RO₂, the results of these two types
260 of RO₂ are shown separately.

261 3.1.1 Non-acyl RO₂

262 In this case non-acyl RO₂ have only three fates, i.e. RO₂+HO₂, RO₂+NO and RO₂+RO₂. The relative
263 importance of these three fates can be shown in a triangle plot (Figure 1). The figure includes data
264 points of OFR185 (including OFR185-iN₂O) and OFR254-70 (including OFR254-70-iN₂O), as well as
265 several typical ambient and chamber studies (Ryerson et al., 2013; Nguyen et al., 2014; Ortega et al.,
266 2014; Martin et al., 2016, 2017; Carlton et al., 2018; Wofsy et al., 2018). Conditions from the FIXCIT
267 campaign (Nguyen et al., 2014) are used to represent chamber studies as they were designed for specific
268 RO₂ fates within the limitations of current high-quality laboratory chambers (Table 2). Bad conditions



269 (in terms of non-tropospheric photolysis) are not shown on these plots because of the lack of
270 experimental interest. The triangle plots for OFR254-7 (including OFR254-7-iN₂O) in the same form
271 (Figure S1a,b) show no qualitative differences from the results of OFR254-70, implying that initial O₃ in
272 OFR254 modes has only minor impacts on RO₂ fate. We see this result not only for well-known non-acyl
273 RO₂ fate, but also for the aspects discussed in the following sections. The similarity between OFR254
274 modes can be explained by the minor effects of a lower O₃ on HO_x at relatively low OHR_{ext} (Peng et al.,
275 2015). Cases at higher OHR_{ext} often have stronger non-tropospheric photolysis (Peng et al., 2016) and
276 hence are more likely to be under bad conditions and are not shown in Figs. 1 and S1a,b. For simplicity,
277 this similarity is not discussed further.

278 An important feature confirmed in Fig. 1 is that OFR-iN₂O modes effectively realize conditions of
279 experimental interest with variable relative importance of RO₂+NO in RO₂ fate (Lambe et al., 2017; Peng
280 et al., 2018). Tuning initially injected N₂O can achieve this goal (Fig. 2). While it is possible to reduce
281 RO₂+HO₂ in OFR185-iN₂O to negligible compared to RO₂+NO by increasing N₂O, this is not possible in
282 OFR254-70-iN₂O due to fast NO oxidation by the large amounts of O₃ added in the reactor. Nevertheless,
283 OFR254-70-iN₂O can still make RO₂+NO dominate over RO₂+HO₂ in RO₂ fate. OFR and chamber cases
284 span a range of ~0–~100% in relative importance of RO₂+NO in RO₂ fate (Fig. 2), suggesting that both
285 chambers and OFRs are able to ensure the atmospheric relevance of RO₂+NO in RO₂ fate.

286 Another important feature that can be easily seen in Fig. 1 is that medium rate RO₂+RO₂ (and
287 hence also RO₂+RO₂ slower than 10⁻¹³ cm³ molecule⁻¹ s⁻¹) are of negligible importance in the fate of RO₂
288 (Fig. 1a,c) in OFR185 (including OFR185-iN₂O), OFR254-70 (under most conditions, including OFR254-
289 70-iN₂O), chambers and the atmosphere. Thus, a very large subset of RO₂ have only minor or negligible
290 contribution from RO₂+RO₂ to their fate. This is already known for ambient RO₂ fate (Ziemann and
291 Atkinson, 2012). The reason why this is also true in OFRs is that while OH is much higher than ambient
292 levels, HO₂ and NO (high-NO conditions only) are also higher. One can easily verify that steady-state RO₂
293 concentrations (see Appendix A for details) would not deviate from ambient levels by orders of
294 magnitude. The reactive fluxes of RO₂+RO₂ in OFRs are thus not substantially different than in the
295 atmosphere, while RO₂+HO₂ and RO₂+NO (high-NO conditions only) are both faster in OFRs because of
296 higher HO₂ and NO. The combined effect is a *reduced* relative importance of RO₂+RO₂ in RO₂ fate in
297 OFRs compared to the atmosphere. The only exception in OFRs occurs at very high VOC precursor
298 concentrations (OHR_{ext} significantly >100 s⁻¹) in OFR254 (Fig. S2), where OH levels are not substantially
299 suppressed due to large amounts of O₃ (Peng et al., 2015). As a result, RO₂ concentration is remarkably
300 increased by strong production and RO₂+RO₂ relative importance increases roughly quadratically and
301 becomes significant.

302 The generally lower relative importance of RO₂+RO₂ in OFRs than in the atmosphere is more
303 obvious for the fate of RO₂ with fast RO₂+RO₂ rate constants (Figs. 1b,d and 3). Although OFRs can
304 reasonably reproduce RO₂ fates in low-VOC ambient environments (e.g. typical pristine and forested
305 areas; Figs. 1b,d and 3) and low-OHR_{ext} chambers, OFR185 cannot achieve relative importance of
306 RO₂+RO₂ significantly larger than 50%, corresponding to higher-VOC environments (e.g. P₁ in Fig. 1) and



307 high-OHR_{ext} chamber experiments (e.g. C₂ and C₅ in Fig. 1; the distribution for C₂ is also shown in Fig. 3).
308 In OFR254-70, a relative importance of RO₂+RO₂ as high as ~90% may be attained (Fig. S3). However,
309 this requires very high OHR_{ext}, which leads to medium (and slower) RO₂+RO₂ showing higher-than-
310 ambient relative importance. In reality, fast RO₂+RO₂ all involve substituted RO₂, which almost certainly
311 arise from and coexist with unsubstituted RO₂ (with slower self-/cross reactions). Therefore, very high
312 OHR_{ext} in OFR254 is not really suitable for attaining dominant RO₂+RO₂ conditions. In OFR185, a higher
313 OHR_{ext} generally also results in a higher RO₂+RO₂ relative importance because of higher RO₂ production
314 (Fig. S3). Nevertheless, higher OHR_{ext} is more likely to lead to risky or bad conditions (Fig. 3; Peng et al.,
315 2016). It should be noted that although it is difficult to reliably achieve RO₂+RO₂ with a relative
316 importance larger than 50% in RO₂ fate in OFRs, the distributions of RO₂+RO₂ relative importance in
317 OFRs seems to be within a factor of 2 of those of field/aircraft campaigns (Fig. 3).

318 In the case of very fast RO₂+RO₂, all features for fast RO₂+RO₂ discussed above are still present
319 (Fig. S1c,d). The only major difference between the results for fast RO₂+RO₂ and very fast RO₂+RO₂ is
320 the significantly higher relative importance of RO₂+RO₂ in RO₂ fate in the latter case, which is expected.
321 In summary, the fast RO₂+RO₂ is not perfectly reproduced in OFRs in terms of relative importance in RO₂
322 fate, but it is significant when this pathway is also important in the atmosphere.

323 The HO_x recycling ratio β (see Sect. 2.3) is one of the key factors determining HO₂ in the OFR
324 model, yet it is not well constrained. Although we make reasonable assumptions for it in the model
325 input (see Section 2.3 for details), a sensitivity study to explore its effects is also performed here. For
326 RO₂ with the fast self-/cross-reaction rate constant, we perform the simulations with the HO_x recycling
327 ratios fixed to a number of values from 0 (radical termination) to 2 (radical proliferation) in lieu of those
328 calculated under the assumptions described in Section 2.3. As expected, the contribution of RO₂+RO₂
329 to RO₂ fate increases monotonically between $\beta=2$ and $\beta=0$ (Fig. S4), as the recycling of the competing
330 reactant HO₂ decreases. Nevertheless, the change in the average RO₂+RO₂ relative importance from $\beta=0$
331 to $\beta=2$ is generally within a factor of 2. Thus, it still holds that the RO₂+RO₂ relative importance in OFRs
332 is generally lower than in the atmosphere. Only at $\beta\sim 0$ may OFR185 theoretically attain a relative
333 importance of RO₂+RO₂ of ~70%, as in the P₁ case (pristine, but relatively high-VOC, Figure S5). Note
334 that $\beta=0$ for all VOC oxidation (including oxidation of intermediates) is extremely unlikely. In OFR254,
335 even if RO₂+RO₂ may contribute up to ~100% to RO₂ fate at very high OHR_{ext} at $\beta=0$, these conditions
336 still also lead to significant RO₂+RO₂ in the fate of RO₂ that self-/cross-react more slowly, which is not
337 atmospherically relevant.

338 3.1.2 Acyl RO₂

339 As described in Section 2.1, the generic acyl RO₂ modeled in this study has the same loss
340 pathways as RO₂ with the fast self-/cross-reaction rate constant, except for RO₂+NO₂, which can be a
341 significant acyl RO₂ loss pathway in OFRs as well as both chambers and atmosphere. When this reaction
342 is included in the simulations of acyl RO₂, it is a minor or negligible loss pathway of RO₂ at low N₂O,
343 while it can be the dominant fate of acyl RO₂ at high N₂O (Fig. 4). In general, the RO₂+NO₂ relative
344 importance increases with initial N₂O. This is always true in OFR254-70-iN₂O between N₂O=0.02% and



345 $\text{N}_2\text{O}=20\%$, while in OFR185- iN_2O , the average relative contribution of RO_2+NO_2 to RO_2 fate starts to
346 decrease at $\text{N}_2\text{O}\sim 10\%$, because RO_2+NO regains some importance. This results from the HO_x
347 suppression caused by high NO_y and strong NO production at high N_2O . Strong NO production increases
348 its concentration and suppresses HO_x under these conditions, limiting the conversion of NO to NO_2 .
349 Because of the strong OH suppression by high NO_y at $\text{N}_2\text{O}\geq 10\%$, these conditions are not desirable (Peng
350 et al., 2018).

351 The only difference between the simulations of acyl RO_2 and of the fast-self-/cross-reacting non-
352 acyl RO_2 is the quasi-irreversible reaction $\text{RO}_2+\text{NO}_2\rightarrow\text{RO}_2\text{NO}_2$, whose effects are revealed by a
353 comparison of the triangle plots of the RO_2 fates in each case (Figs. 1b,d and S6). RO_2+NO_2 is clearly
354 dominant in acyl RO_2 fate in OFRs as long as RO_2+NO plays some role (not necessarily under high- NO
355 conditions). In OFR185- iN_2O , the relative importance of RO_2+RO_2 in the sum of the HO_2 , NO and RO_2
356 pathways is reduced (Fig. S6a), compared to that of non-acyl RO_2 with the fast RO_2+RO_2 (Fig. 1b),
357 because RO_2+NO_2 decrease acyl RO_2 concentration. Such a decrease is not significant in OFR254-70-
358 iN_2O (Fig. S6b, compared to Fig. 1d), since for non-acyl RO_2 , it is already stored in the form of RO_2NO_2
359 as RO_2 reservoir. In other words, the high initial O_3 greatly accelerates NO -to- NO_2 oxidation, and shifts
360 the equilibrium $\text{RO}_2+\text{NO}_2\leftrightarrow\text{RO}_2\text{NO}_2$ far to the right even for non-acyl RO_2 .

361 RO_2+NO_2 is an inevitable sink of most acyl RO_2 in high- NO_x OFRs. Its contribution to acyl RO_2 fate
362 in OFRs is often higher than in urban atmospheres, where the relative amounts of NO and NO_2 vary
363 overtime. At midday, most NO is usually oxidized to NO_2 in urban atmospheres and RO_2+NO_2 dominates
364 acyl RO_2 fate, as in high- NO_x OFRs. During morning rush hours and/or near major NO sources, NO may
365 be significantly more abundant than NO_2 and RO_2+NO is likely the dominant acyl RO_2 loss pathway,
366 which cannot be simulated in OFRs with the current range of techniques.

367 Acyl RO_2 are not the dominant type among RO_2 s under most conditions in OFRs, chambers and
368 the atmosphere, since their formation usually requires multistep (at least 2 steps) oxidation via specific
369 pathways leading to an oxidized end group (i.e. aldehyde and then acylperoxy). However, acyl RO_2 can
370 still be a major (very roughly 1/3) source of RO_2 at ages of several hours or higher according to
371 estimations made using the GECKO-A model in urban and forested atmospheres. Therefore, acyl RO_2
372 chemistry in high- NO OFR can significantly deviate from that in an urban atmosphere with NO
373 dominating NO_x , and can be relevant to an urban atmosphere with NO_2 dominating NO_x . On the other
374 hand, a few theoretical studies suggested that H-abstraction by the acylperoxy radical site from
375 hydroperoxy groups close to the acylperoxy site in multifunctional acyl RO_2 may be extremely fast
376 (Jørgensen et al., 2016; Knap and Jørgensen, 2017). If these theoretical predictions are sufficiently
377 accurate, these acyl RO_2 may exclusively undergo intramolecular H-shift to form non-acyl RO_2 or other
378 radicals and prevent RO_2+NO_2 from occurring even at very high (ppm-level) NO_2 . However, this type of
379 RO_2 is structurally specific and may not have strong impacts on the overall acyl RO_2 chemistry.

380 3.2 Simulations with all significant pathways

381 Since RO_2 isomerization does not significantly affect the generic RO_2 concentration, the two RO_2
382 fates that were recently found to be potentially important, i.e. RO_2+OH and RO_2 isomerization, can be



383 discussed separately.

384 3.2.1 RO₂+OH

385 In the troposphere, RO₂+OH is a minor (at low NO) or negligible (at high NO) RO₂ loss pathway
386 (Fittschen et al., 2014; Assaf et al., 2016; Müller et al., 2016), as its rate constant is roughly an-order-of-
387 magnitude higher than that of RO₂+HO₂ (Table 1) while ambient OH concentration is on average 2-
388 orders-of-magnitude lower than that of HO₂ (Mao et al., 2009; Stone et al., 2012; Fig. 5). We will not
389 discuss RO₂+OH in the high-NO cases in detail. Simply put, the relative importance of RO₂+OH is
390 generally negatively correlated with input N₂O in OFR-iN₂O, as NO_x suppresses OH and the relative
391 importance of RO₂+NO increases. Below, we focus on low-NO (actually, for simplicity, zero-NO)
392 conditions.

393 At N₂O=0, it would be ideal if an HO₂-to-OH ratio identical to the ambient values was realized in
394 OFRs. In OFR185 cases with medium RO₂+RO₂, HO₂-to-OH ratio around 100 occurs at a combination of
395 low H₂O (on the order of 0.1%), low F185 (on the order of 10¹¹ photons cm⁻² s⁻¹), and medium OHR_{ext}
396 (10–100 s⁻¹); and also at medium F185 (~10¹² photons cm⁻² s⁻¹) combined with very high OHR_{ext} (~1000
397 s⁻¹, Fig. S7). Under both sets of conditions, relatively high external OH reactants suppress OH, whose
398 production is relatively weak, and convert some OH into HO₂ through HO_x recycling in organic oxidation
399 (e.g. via alkoxy radical chemistry). The reason why such an OH-to-HO₂ conversion is needed to attain an
400 ambient-like HO₂-to-OH ratio is that OFR185 is unable to achieve this via the internal (mainly assisted
401 by O₃) interconversion of HO_x. This inability is most evident when F185 (10¹³–10¹⁴ photons cm⁻² s⁻¹) and
402 H₂O (on the order of 1%) are high and OHR_{ext} is low (<~10 s⁻¹; Fig. S7). Under these conditions, OH
403 production by H₂O photolysis is so strong that the HO₂-to-OH ratio is lowered to ~1, since OH and H
404 (which recombines with O₂ to form HO₂) are produced in equal amounts from H₂O photolysis. As the
405 RO₂+OH rate constant is only roughly 1-order-of-magnitude higher than that for RO₂+HO₂, slightly lower
406 HO₂-to-OH ratios (e.g. ~30) suffice to keep RO₂+OH minor in this case. A combination of UV and H₂O
407 that are not very high and a moderate OHR_{ext} that is able to convert some OH to HO₂ and somewhat
408 elevate the HO₂-to-OH ratio results in minor relative importance RO₂+OH (Figs. S7 and S8).

409 In OFR254-70, it is more difficult to reach an HO₂-to-OH ratio of ~100, which can only be realized
410 at a combination of very low H₂O and F254 (~0.07% and ~5x10¹³ photons cm⁻² s⁻¹, respectively) and very
411 high OHR_{ext} (~1000 s⁻¹). This is mainly due to high O₃ in OFR254-70, which controls the HO_x
412 interconversion through HO₂+O₃→OH+2O₂ and OH+O₃→HO₂+O₂ and makes both OH and HO₂ more
413 resilient to changes due to OHR_{ext} (Peng et al., 2015). Even without H₂O photolysis at 185 nm as a major
414 HO₂ source, the HO_x interconversion controlled by O₃ in OFR254-70 still brings HO₂-to-OH ratio to ~1 in
415 the case of minimal external perturbation (see the region at the highest H₂O and UV and OHR_{ext}=0 in
416 the OFR254-70 part of Fig. S7). This ratio cannot be easily elevated in OFR254-70 because of the
417 resilience of OH to suppression for this mode (Peng et al., 2015). Thus, this ratio is relatively low (<30)
418 under most conditions (Fig. S7), and consequently (and undesirably), RO₂+OH is a major RO₂ fate in
419 OFR254-70. There is an exception at relatively low H₂O and UV with very high OHR_{ext} (Fig. S8), however
420 these conditions are undesirable in terms of non-tropospheric organic photolysis (Peng et al., 2016).



421 Only the results of RO₂ with the medium RO₂+RO₂ are discussed in this subsection. Those of RO₂
422 with the fast RO₂+RO₂ are not shown as they are not qualitatively different. In OFR185, for the fast-self-
423 /cross-reacting RO₂, RO₂+RO₂ is relatively important at high OHR_{ext} (>~100 s⁻¹; Fig. S3), while RO₂+OH is
424 a major RO₂ fate at low OHR_{ext} (generally on the order of 10 s⁻¹ or lower) and relatively high H₂O and UV
425 (Fig. S8). These two ranges of conditions are relatively far away from each other, and hence there is no
426 condition under which RO₂+RO₂ and RO₂+OH are both major pathways that compete, which simplifies
427 understanding RO₂ fate. However, in OFR254-70, some conditions may lead to both significant RO₂+RO₂
428 (for the fast-self-/cross-reacting RO₂) and RO₂+OH (e.g. H₂O~0.5%, F254~1x10¹⁵ photons cm⁻² s⁻¹ and
429 OHR_{ext}~100 s⁻¹). Nevertheless, as long as RO₂+OH plays a major role, these conditions do not bear much
430 experimental interest and thus do not need to be discussed in detail.

431 3.2.2 RO₂ isomerization

432 RO₂ isomerization is a first-order reaction. For this type of reactions to occur, RO₂ does not need
433 any other species but only a sufficiently long lifetime against all other reactants combined, as most RO₂
434 isomerization rate constants are <10 s⁻¹. Radical (OH, HO₂, NO etc.) concentrations in OFRs are much
435 higher than ambient levels and may shorten RO₂ lifetimes compared to those in the troposphere.
436 Possibly reduced RO₂ lifetimes naturally raise concerns over the potentially diminished importance of
437 RO₂ isomerization in OFRs.

438 In this section we examine generic RO₂ lifetimes against all reactions (calculated without RO₂
439 isomerization taken into account) in OFR (including OFR-iN₂O) cases (for the medium RO₂+RO₂ case) and
440 compare them with the RO₂ lifetimes in recent major field/aircraft campaigns in relatively clean
441 environments and a field campaign in an urban area (CalNex-LA), as well as a low-NO chamber
442 experiment (Fig. 6). Indeed, RO₂ lifetime in clean ambient cases and in chambers with near-ambient
443 radical levels are generally much longer than those in OFRs. The RO₂ lifetime distribution of the explored
444 good and risky cases in OFR254-70 (including OFR254-70-iN₂O) barely overlaps with the ambient and
445 chamber cases, while in OFR185 (including OFR185-iN₂O), RO₂ lifetime can be as long as ~10 s, which is
446 longer than in urban areas and roughly at the lower end of the range of ambient RO₂ lifetime in clean
447 environments (Fig. 6). The longest RO₂ lifetime in OFR185 occurs at very low F185 (on the order of 10¹¹
448 photons cm⁻² s⁻¹) and H₂O (~0.1%; Fig. S9), where HO_x is low. In OFR254-70, for RO₂ to survive for ~10 s,
449 in addition to very low UV and H₂O, high OHR_{ext} is also needed (Fig. S9). High-OHR_{ext} conditions in
450 OFR254-70 cause OH suppression and a decrease in HO_x concentration, and hence result in relatively
451 long RO₂ lifetimes. However, the strong OH suppression is likely to give bad conditions (high contribution
452 of non-tropospheric photolysis).(Peng et al., 2016) Low-OHR_{ext} conditions do not lead to long RO₂
453 lifetimes in OFR254-70 even at very low F254 and H₂O, since O₃-assisted HO_x recycling prevents a very
454 low HO_x level even if HO_x primary production is low.(Peng et al., 2015)

455 An RO₂ lifetime (without RO₂ isomerization included) of 10 s leads to a relative importance of
456 isomerization of 50% in the total fate (including all loss pathways) of RO₂ with an isomerization rate
457 constant of 0.1 s⁻¹, which is a typical order of magnitude for isomerization rate constants of
458 multifunctional RO₂ with hydroxyl and hydroperoxy substituents (Fig. 6; Crouse et al., 2013; D'Ambro



459 et al., 2017; Praske et al., 2018). Although a 50% relative importance of isomerization under some OFR
460 conditions is still lower than those in relatively low-NO ambient environments and low-NO chambers,
461 this relative importance should certainly be deemed major and far from negligible as some have
462 speculated (Crouse et al., 2013). Other monofunctional RO₂ (with peroxy radical site only) and
463 bifunctional RO₂ with peroxy radical site and a carbonyl group isomerize so slowly ($\sim 0.001\text{--}0.01\text{ s}^{-1}$) that
464 their isomerizations are minor or negligible loss pathways in the atmosphere, chambers and OFRs with
465 RO₂ lifetimes around 10 s (Fig. 6). Isomerizations of other types of multifunctional RO₂ (e.g.
466 multifunctional acyl RO₂ with hydroxyl and hydroperoxy substituents at favorable positions) are
467 extremely fast (rate constants up to 10^6 s^{-1} ; Jørgensen et al., 2016; Knap and Jørgensen, 2017) and
468 always dominate in their fates in the relatively low-NO atmosphere and chambers and OFRs with RO₂
469 lifetimes around 10 s.

470 In the discussion about RO₂ isomerization above (as in the RO₂+OH exploration in Section 3.2.1),
471 we only examine low-NO (or zero-NO for simplicity) conditions with medium RO₂+RO₂. In high-NO
472 environments, e.g. polluted urban atmospheres with NO of at least ~ 10 ppb and high-NO OFRs in the
473 iN₂O modes, RO₂ lifetime is so short that isomerization is no longer a major fate for any but the most
474 rapidly isomerizing multifunctional RO₂ discussed above. NO measured in Los Angeles during the
475 CalNex-LA campaign (Ortega et al., 2016) was only ~ 1 ppb, which would allow RO₂ to survive for a
476 few seconds and isomerize (Fig. 6), even in an urban area.

477 The OFR simulations for the discussions about RO₂ isomerization are the same as those
478 conducted to study RO₂+OH, i.e. the ones with the medium RO₂+RO₂ and RO₂+OH included. For fast RO₂
479 self-/cross-reaction cases, RO₂ lifetimes may be significantly shorter than for RO₂ with the medium self-
480 /cross-reaction rate constant at high OHR_{ext} ($> \sim 100\text{ s}^{-1}$) in OFR185 (Fig. S3). These high-OHR_{ext} conditions
481 are likely to be risky or bad (of little experimental interest) (Peng et al., 2016) and thus do not need to
482 be discussed further in detail. OFR254-70 (a zero-NO mode) does not generate good or risky (of at least
483 some experimental interest in terms of non-tropospheric organic photolysis) conditions also leading to
484 low-NO-atmosphere-relevant RO₂ lifetimes (Fig. 6). RO₂ with faster self-/cross-reaction rate constants
485 have even shorter lifetimes in OFR254-70 and will not be discussed further.

486 3.3 Guidelines for OFR operation

487 In this subsection we discuss OFR operation guidelines for atmospherically relevant RO₂ chemistry,
488 with a focus on OFR185 and OFR254 (zero-NO modes). Since RO₂+HO₂ and RO₂+NO both can vary from
489 negligible to dominant RO₂ fate in OFRs, chambers and the atmosphere (Figs. 1 and 2), these two
490 pathways are not a concern in OFR atmospheric relevance considerations. Neither is the RO₂+RO₂ a
491 major concern. Medium or slower RO₂+RO₂ is minor or negligible in the atmosphere and chambers, as
492 well as in OFRs, as long as high OHR_{ext} is avoided in OFR254 (Fig. S2). Fast RO₂+RO₂ is somewhat less
493 important in OFRs than in the atmosphere (Figs. 1b,d and 3), but is still qualitatively atmospherically
494 relevant, given the uncertainties associated with the HO_x recycling ratios of various reactive systems
495 and the huge variety of RO₂ types (and hence RO₂+RO₂ rate constants).

496 Accordingly, we focus on the atmospheric relevance of RO₂+OH and RO₂ isomerization, i.e. their



497 relative contributions close to ambient values. Under typical high-NO conditions, RO₂+NO dominates
498 RO₂ fate and RO₂+OH is negligible. High NO also shortens RO₂ lifetime enough to effectively inhibit RO₂
499 isomerization. Both the dominance of RO₂+NO and the inhibition of RO₂ isomerization also occur in the
500 atmosphere and in chambers, so high-NO OFR operation (typically NO>10 ppb) represents these
501 pathways realistically. Some care is, however, required with the RO₂+OH and RO₂ isomerization
502 pathways at low NO. Since RO₂+HO₂ in OFRs is always a major RO₂ fate at low NO and RO₂+RO₂ are
503 generally not problematic, RO₂+OH and RO₂+HO₂ can be kept atmospherically relevant as long as HO₂-
504 to-OH ratio is close to 100 (the ambient average). In addition, RO₂ lifetime (calculated without RO₂
505 isomerization taken into account) should be at least around 10 s.

506 Practically, OH production should be limited to achieve this goal. Too strong OH production at high
507 H₂O and UV can elevate OH and HO₂ concentrations, which shortens RO₂ lifetime, and decreases the
508 HO₂-to-OH ratio to ~1 (see Sect. 3.2.1). OH production is roughly proportional to both H₂O and UV (Peng
509 et al., 2015), so can be limited by reducing either or both. However, H₂O and UV have different effects
510 on non-tropospheric organic photolysis. At a certain OHR_{ext}, OH production rate roughly determines OH
511 concentration in OFRs. Reducing UV decreases both OH and UV roughly proportionally (Peng et al.,
512 2015), and hence changes in F185_{exp}/OH_{exp} and F254_{exp}/OH_{exp} are small (Peng et al., 2016); i.e. non-
513 tropospheric organic photolysis does not become significantly worse if UV is reduced. By contrast, if H₂O
514 is reduced without also decreasing UV, F185_{exp}/OH_{exp} and F254_{exp}/OH_{exp} both increase, signifying
515 stronger relative importance of non-tropospheric photolysis. Therefore, reducing UV is strongly
516 preferred as an OH production limitation method, and is effective in making both RO₂+OH and RO₂
517 isomerization more atmospherically relevant.

518 To further explore the effects of UV reduction on the RO₂+OH (Fig. 5) and RO₂ isomerization (Fig.
519 6) pathways, we divide our OFR case distributions into higher-UV and lower-UV classes, with the
520 boundary being the mid-level (in logarithmic scale) UV in the explored range. The distributions for
521 lower-UV conditions (solid lines in Figs. 5 and 6) are clearly closer to the ambient cases (i.e. HO₂-to-OH
522 ratio closer to 100, smaller RO₂+OH relative importance and longer RO₂ lifetime).

523 Since OFR254 is unable to achieve conditions with both at least some experimental interest (i.e.
524 with sufficiently low non-tropospheric photolysis) and atmospherically relevant RO₂ lifetime, we now
525 discuss preferable conditions for OFR185 only. As F185 close to or lower than 10¹² photons cm⁻² s⁻¹ is
526 needed for RO₂ lifetime to be around 10 s or longer (Fig. S9), the OH concentration under preferable
527 conditions for atmospherically relevant RO₂ chemistry (~10⁹ molecules cm⁻³ or lower) is much lower
528 than the maximum that OFR185 can physically reach (~10¹⁰–10¹¹ molecules cm⁻³). Furthermore, lower
529 OH production leads to higher susceptibility to OH suppression by external OH reactants (Peng et al.,
530 2015), which can create non-tropospheric photolysis problems (Peng et al., 2016). We thus recommend
531 as high H₂O as possible to maintain practically high OH while allowing lower UV to limit the importance
532 of non-tropospheric organic photolysis.

533 The performance of various OFR185 conditions at high H₂O (2.3%) is illustrated in Fig. 7 as a
534 function of F185 and OHR_{ext}. The three criteria for the performance, i.e. RO₂ lifetime (calculated without



535 RO₂ isomerization considered), relative importance of RO₂+OH and log(F254_{exp}/OH_{exp}) (a measure of
536 254 nm non-tropospheric photolysis, which is usually worse than that at 185 nm; Peng et al., 2016) are
537 shown. At F185 of ~10¹¹–10¹² photons cm⁻² s⁻¹ and OHR_{ext} around or lower than 10 s⁻¹, all three criteria
538 are satisfied. Since UV (and hence OH production) is relatively low, a low OHR_{ext} (~10 s⁻¹) is required to
539 avoid heavy OH suppression and keep conditions good (green area in the bottom panel of Fig. 7).
540 Nevertheless, risky conditions [log(F254_{exp}/OH_{exp})<7; light red area in the bottom panel of Fig. 7] may
541 also bear some experimental conditions depending on the type of VOC precursors (specifically on their
542 reactivity toward OH and their photolability at 185 and 254 nm, and the same quantities for their
543 oxidation intermediates; Peng et al., 2016; Peng and Jimenez, 2017). Thus, higher OHR_{ext} (up to ~100 s⁻¹)
544 may also be considered in OFR experiments with some precursors (e.g. alkanes). In practice, the
545 preferred conditions may require F185 even lower than that our lowest simulated lamp setting (Li et al.,
546 2015). Such a low F185 may be realized e.g. by partially blocking 185 nm photons using non-transparent
547 lamp sleeves with evenly placed holes that allow some 185 nm transmission.

548 Under these preferred conditions, OH concentration in OFR185 is ~10⁹ molecules cm⁻³, equivalent
549 to a photochemical age of ~1 eq. d for a typical residence time of 180 s. This is much shorter than ages
550 corresponding to the maximal oxidation capacity of OFRs (usually eq. weeks or months; Peng et al.,
551 2015) but it is similar to the ages of the maximal organic aerosol formation in OFRs processing ambient
552 air (Tkacik et al., 2014; Ortega et al., 2016; Palm et al., 2016). We show the maximal SOA formation case
553 in the OFR185 experiments in the BEACHON-RoMBAS campaign in the Rocky Mountains (Palm et al.,
554 2016) as an example (Figs. 5 and 6). During the campaign, relative humidity was high (>60% in most of
555 the period), OHR_{ext} was estimated to be relatively low (~15 s⁻¹) in this forested area, and UV in the OFR
556 was limited in the case of the maximal SOA formation age (~0.7 eq. d). All these physical conditions
557 were favorable for atmospherically relevant RO₂ fate (Figs. 5 and 6). RO₂+OH was minor in this case and
558 the relative importance of RO₂ isomerization in RO₂ fate in the OFR was within a factor of ~2 of that in
559 the atmosphere for all RO₂ (regardless of isomerization rate constant) during the BEACHON-RoMBAS
560 campaign (Fig. 6). The effect of UV on the relative importance of RO₂ isomerization for this example is
561 also illustrated in Fig. 6. In the sensitivity case with a lower age, a lower UV results in a larger
562 contribution of isomerization to RO₂ fate, while the relative importance of RO₂ isomerization is lower in
563 a sensitivity case with an age 3 times of that of the maximal SOA formation. In an extreme sensitivity
564 case with the highest UV in the range of this study (with an age of 4 eq. mo), RO₂ isomerization becomes
565 minor or negligible for all RO₂ except extremely rapidly isomerizing ones.

566 The discussions above indicate that the atmospheric relevance of gas-phase RO₂ chemistry in OFRs
567 deteriorates as the photochemical age over the whole residence time (180 s) increases. To reach longer
568 ages, longer residence times (with UV being still low) can be adopted. However, OFR residence times >
569 10 min tend to be limited by the increasing importance of wall losses (Palm et al., 2016). As a result,
570 longer residence times can only increase photochemical age in OFRs up to about a week. This implies
571 that in OFR cases with ages much higher than that of maximal SOA formation (corresponding to the
572 heterogeneous oxidation stage of SOA), the atmospheric relevance of gas-phase RO₂ chemistry in the



573 SOA formation stage (before the age of maximal SOA formation) often cannot be ensured. However,
574 under those conditions typically new SOA formation is not observed, and the dominant process
575 affecting OA is heterogeneous oxidation of the pre-existing OA (Palm et al., 2016). If the heterogeneous
576 oxidation of the newly formed SOA is of interest, a two-stage solution may be required. Lower UV can
577 be used in the SOA formation stage to keep the atmospheric relevance of the gas-phase chemistry, while
578 high UV can be used in the heterogeneous aging stage to reach a high equivalent age. The latter
579 approach is viable since heterogeneous oxidation of SOA by OH is slow and particle-phase chemistry is
580 not strongly affected by gas-phase species except OH, when OH is very high (Richards-Henderson et al.,
581 2015, 2016; Hu et al., 2016). This two-stage solution may be realized through a cascade-OFR system or
582 UV sources at different intensities within an OFR (e.g. spliced lamps).

583 Praske et al. (2018) measured RO₂ isomerization rate constants at 296 and 318 K and observed an
584 increase in the rate constants by a factor of ~5 on average. A 15 K temperature increase in OFRs would
585 lead to RO₂ isomerization being accelerated by a factor of ~3, while other major gas-phase radical
586 reactions have weak or no temperature-dependence. As a consequence, the relative importance of RO₂
587 isomerization in RO₂ fate in OFRs can be elevated and closer to atmospheric values (Fig. 6). Nevertheless,
588 a 15 K increase in temperature may also result in some OA evaporation (Nault et al., 2018).

589 As discussed above, high H₂O, low UV and low OHR_{ext} are recommended for keeping the
590 atmospheric relevance of RO₂ chemistry in OFRs. These three requirements are also part of the
591 requirements for attaining good high-NO conditions in OFR185-iNO (the OFR185 mode with initial NO
592 injection; Peng and Jimenez, 2017). In addition to these three, an initial NO of several tens of ppb is also
593 needed to obtain a good high-NO condition in OFR185-iNO. Under these conditions, RO₂+NO dominates
594 over RO₂+HO₂, and hence RO₂+OH; UV is low, the photochemical age is typically ~1 eq. d, and RO₂
595 lifetime can be a few seconds. Therefore, these conditions are a good fit for studying the environments
596 in relatively clean urban areas, such as Los Angeles during CalNex-LA (Ortega et al., 2016), where NO is
597 high enough that the dominant bimolecular fate of RO₂ is RO₂+NO but low enough to maintain RO₂
598 lifetimes that allow most common RO₂ isomerizations.

599 As RO₂ fate in OFRs is a highly complex problem and it can be tricky to find suitable physical
600 conditions to simultaneously achieve experimental goals and keep the atmospheric relevance of the
601 chemistry in OFRs, we provide here an OFR RO₂ Fate Estimator (in Supplement) to qualitatively aid
602 experimental planning. The OFR RO₂ Fate Estimator couples the OFR Exposure Estimator (Peng et al.,
603 2016, 2018) to a General RO₂ Fate Estimator (also in Supplement, see Fig. S10 for a screenshot of its
604 layout). The OFR Exposure Estimator updated in this study also contains estimation equations for the
605 HO₂-to-OH ratio in OFR185 (in OFR254, RO₂ fate is always atmospherically irrelevant at low NO, while
606 at high NO, RO₂+NO dominates and a detailed RO₂ fate analysis is no longer needed). In the General RO₂
607 Fate Estimator, all RO₂ reactant concentrations and all RO₂ loss pathway rate constants can be specified.
608 Thus the General RO₂ Fate Estimator can also be applied to the atmosphere and chamber experiments,
609 in addition to OFRs. When applied to OFRs, the General RO₂ Fate Estimator is provided by the OFR RO₂
610 Fate Estimator with quantities estimated in the OFR Exposure Estimator (e.g. OH and NO). RO₂



611 concentration and fate are calculated according to Appendix A in the RO₂ Fate Estimators.

612 **4 Conclusions**

613 We investigated RO₂ chemistry in OFRs with an emphasis on its atmospheric relevance. All
614 potentially major loss pathways of RO₂, i.e. reactions of RO₂ with HO₂, NO and OH, that of acyl RO₂ with
615 NO₂, self-/cross-reactions of RO₂ and RO₂ isomerization, were studied and their relative importance in
616 RO₂ fate were compared to those in the atmosphere and chamber experiments. OFRs were shown to
617 be able to tune the relative importance of RO₂+HO₂ vs. RO₂+NO by injecting different amounts of N₂O.
618 For many RO₂ (including all unsubstituted non-acyl RO₂ and substituted secondary and tertiary RO₂),
619 their self-reactions and the cross-reaction between them are minor or negligible in the atmosphere and
620 chambers. This is also the case in OFR185 (including OFR185-iN₂O) and OFR254-iN₂O, however those
621 RO₂ self-/cross-reactions can be important at high precursor concentrations (OHR_{ext}>100 s⁻¹) in OFR254.
622 For substituted primary RO₂ and acyl RO₂, their self-/cross-reactions (including the ones with RO₂ whose
623 self-reaction rate constants are slower) can play an important role in RO₂ fate in the atmosphere and
624 chambers, and may also be major RO₂ loss pathways in OFRs, although they are somewhat less
625 important in OFRs than in the atmosphere. Acylperoxy nitrates are the dominant sink of acyl RO₂ at high
626 NO_x in OFRs, while only a minor reservoir of acyl RO₂ in the atmosphere under most conditions except
627 in urban atmospheres, where acylperoxy nitrate formation can be the dominant acylperoxy loss
628 pathway when most NO is oxidized to NO₂. In chambers, most acyl RO₂ can be stored in the form of
629 acylperoxy nitrates if NO₂ is very high (hundreds of ppb to ppm level).

630 Under typical high-NO conditions, RO₂+NO dominates RO₂ fate and RO₂ lifetime is too short to
631 allow most RO₂ isomerizations, regardless of whether in the atmosphere, chambers or OFRs, thus raising
632 no concern over the atmospheric relevance of the OFR RO₂ chemistry. However, under low-NO
633 conditions, OFR254 cannot yield any physical conditions leading to sufficiently long RO₂ lifetime for its
634 isomerization because of the high radical levels and their resilience to external perturbations in OFR254.
635 In OFR185 with strong OH production (and hence high OH), RO₂+OH and RO₂ isomerization may strongly
636 deviate from the atmosphere (becoming important and negligible, respectively, for relatively rapidly
637 isomerizing RO₂). To attain both atmospherically relevant VOC and RO₂ chemistries, OFR185 requires
638 high H₂O, low UV and low OHR_{ext}, which conditions ensure minor or negligible RO₂+OH and a relative
639 importance of RO₂ isomerization in RO₂ fate in OFRs within x~2 of that in the atmosphere but limit the
640 maximal photochemical age that can be reached to a few eq. days. This age roughly covers SOA
641 formation in ambient air up to its maximum. To reach a much higher age for studying SOA
642 functionalization/fragmentation by heterogeneous oxidation, a sequence of low-UV SOA formation
643 followed by a high UV condition (in the same reactor or in cascade reactors) would be needed. High
644 H₂O, low UV and low OHR_{ext} in the OFR185-iNO mode can achieve conditions relevant to clean urban
645 atmosphere, i.e. high-NO but not sufficiently high to inhibit common RO₂ isomerization.

646 Finally, RO₂ chemistry is not only highly complex but also plays a central and instrumental role in
647 atmospheric chemistry, in particular VOC oxidation and SOA formation. For all experiments conducted
648 with atmospheric chemistry simulation apparatus (chambers, flow reactors etc.), an atmospherically



649 relevant RO₂ chemistry is crucial to meaningful experimental results. However, most literature studies
 650 did not publish experimental data that are sufficient for estimating RO₂ fate. The FIXCIT chamber
 651 experiment campaign is one of the few exceptions where comprehensive data were reported (Nguyen
 652 et al., 2014) and used for the RO₂ fate analysis in the present work. We recommend measuring and/or
 653 estimating and reporting OH, HO₂, NO, NO₂ and OHR_{VOC} (or initial precursor composition at least)
 654 whenever possible, for all future atmospheric laboratory and field experiments for organic oxidation to
 655 facilitate the analysis of RO₂ fate and the evaluation of its atmospheric relevance.

656

657 **Appendix A: Steady-state approximation for generic RO₂**

658 The production rate of a generic RO₂ is almost identical to the VOC consumption rate, since the
 659 second step of the conversion chain VOC → R → RO₂ is extremely fast. Therefore, the generic RO₂
 660 production rate, *P*, can be expressed as follows:

$$661 \quad P = \sum_i k_i c_i \cdot \text{OH} = \text{OHR}_{\text{VOC}} \cdot \text{OH} \quad (\text{A1})$$

662 where OH is OH concentration and *c_i* and *k_i* are respectively the concentration and the reaction rate
 663 constant with OH of the *i*th VOC. OHR_{VOC} is the total OHR due to VOC and equal to $\sum_i k_i c_i$ by definition.

664 For the generic RO₂ loss rate, the reactions of RO₂ with HO₂, NO, RO₂, NO₂ (for acyl RO₂ only) and
 665 OH are considered. Isomerization generally does not lead to a total RO₂ concentration decrease and is
 666 thus not included in its loss rate. Then the RO₂ loss rate is

$$667 \quad L = k_{\text{HO}_2} \text{RO}_2 \cdot \text{HO}_2 + k_{\text{NO}} \text{RO}_2 \cdot \text{NO} + 2k_{\text{RO}_2} \text{RO}_2 \cdot \text{RO}_2 + k_{\text{NO}_2} \text{RO}_2 \cdot \text{NO}_2 + k_{\text{OH}} \text{RO}_2 \cdot \text{OH} \quad (\text{A2})$$

668 where RO₂, HO₂, NO, NO₂ and OH are the concentrations of corresponding species and *k_A* (*A* = RO₂, HO₂,
 669 NO, NO₂ and OH) is the reaction rate constant of RO₂ with *A*. For non-acyl RO₂, the term *k_{NO₂}* RO₂ · NO₂
 670 is not included; for cases with well-known pathways only (RO₂+HO₂, RO₂+RO₂, RO₂+NO and RO₂+NO₂;
 671 see Section 3.1), the term *k_{OH}* RO₂ · OH is excluded. *k_{RO₂}* needs to be given a value (which may be the
 672 main levels of RO₂ self-/cross-reaction rate constants in this study, 1x10⁻¹³ and 1x10⁻¹¹ cm³ molecule⁻¹ s⁻¹,
 673 or other values depending on the RO₂ type).

674 At the steady state, *P* and *L* are equal. For an ambient/chamber setting, OH, HO₂, NO, NO₂ and
 675 OHR_{VOC} are often measured or known. In this case, simultaneously considering Eqs. A1 and A2 yields a
 676 quadratic equation of RO₂ concentration (the only unknown). Then generic RO₂ concentration can be
 677 easily obtained by solving this equation:

$$678 \quad \text{RO}_2 = \left(-K + \sqrt{K^2 + 8k_{\text{RO}_2} \cdot \text{OHR}_{\text{VOC}} \cdot \text{OH}} \right) / (4k_{\text{RO}_2}) \quad (\text{A3})$$

679 where $K = k_{\text{HO}_2} \text{HO}_2 + k_{\text{NO}} \text{NO} + k_{\text{NO}_2} \text{NO}_2 + k_{\text{OH}} \text{OH}$.

680

681 **Conflicts of interest**

682 There are no conflicts to declare.

683

684 **Acknowledgements**

685 This work was partially supported by grants EPA STAR 83587701-0, NSF AGS-1740610, NSF AGS-1822664,
 686 NASA NNX15AT96G, and DOE(BER/ASR) DE-SC0016559. We thank the following individuals for providing



687 data from atmospheric field studies: Tran Nguyen and Jordan Krechmer (FIXCIT), William Brune (SOAS
688 and ATom), Pedro Campuzano-Jost (ATom), Daun Jeong and Saewung Kim (GoAmazon). We are also
689 grateful to John Crouse, Joel Thornton, Paul Ziemann, Dwayne Heard, Paul Wennberg, Andrew Lambe
690 and William Brune for useful discussions and Donna Sueper for her assistance in the development of
691 the RO₂ Fate Estimator. NCAR is sponsored by the National Science Foundation. EPA has not reviewed
692 this manuscript and thus no endorsement should be inferred.
693

694 **References**

- 695 Assaf, E., Song, B., Tomas, A., Schoemaeker, C. and Fittschen, C.: Rate Constant of the Reaction between
696 CH₃O₂ Radicals and OH Radicals Revisited, *J. Phys. Chem. A*, 120(45), 8923–8932,
697 doi:10.1021/acs.jpca.6b07704, 2016.
- 698 Assaf, E., Tanaka, S., Kajii, Y., Schoemaeker, C. and Fittschen, C.: Rate constants of the reaction of C₂–
699 C₄ peroxy radicals with OH radicals, *Chem. Phys. Lett.*, 684, 245–249, doi:10.1016/j.cplett.2017.06.062,
700 2017a.
- 701 Assaf, E., Sheps, L., Whalley, L., Heard, D., Tomas, A., Schoemaeker, C. and Fittschen, C.: The Reaction
702 between CH₃O₂ and OH Radicals: Product Yields and Atmospheric Implications, *Environ. Sci. Technol.*,
703 51(4), 2170–2177, doi:10.1021/acs.est.6b06265, 2017b.
- 704 Assaf, E., Schoemaeker, C., Vereecken, L. and Fittschen, C.: Experimental and theoretical investigation
705 of the reaction of RO₂ radicals with OH radicals: Dependence of the HO₂ yield on the size of the alkyl
706 group, *Int. J. Chem. Kinet.*, 50(9), 670–680, doi:10.1002/kin.21191, 2018.
- 707 Atkinson, R. and Arey, J.: Atmospheric degradation of volatile organic compounds., *Chem. Rev.*, 103(12),
708 4605–38, doi:10.1021/cr0206420, 2003.
- 709 Aumont, B., Szopa, S. and Madronich, S.: Modelling the evolution of organic carbon during its gas-phase
710 tropospheric oxidation: development of an explicit model based on a self generating approach, *Atmos.*
711 *Chem. Phys.*, 5(9), 2497–2517, doi:10.5194/acp-5-2497-2005, 2005.
- 712 Berndt, T., Scholz, W., Mentler, B., Fischer, L., Herrmann, H., Kulmala, M. and Hansel, A.: Accretion
713 Product Formation from Self- and Cross-Reactions of RO₂ Radicals in the Atmosphere, *Angew. Chemie*
714 *Int. Ed.*, 57(14), 3820–3824, doi:10.1002/anie.201710989, 2018.
- 715 Bossolasco, A., Faragó, E. P., Schoemaeker, C. and Fittschen, C.: Rate constant of the reaction between
716 CH₃O₂ and OH radicals, *Chem. Phys. Lett.*, 593(2014), 7–13, doi:10.1016/j.cplett.2013.12.052, 2014.
- 717 Burkholder, J. B., Sander, S. P., Abbatt, J., Barker, J. R., Huie, R. E., Kolb, C. E., Kurylo, M. J., Orkin, V. L.,
718 Wilmouth, D. M. and Wine, P. H.: Chemical Kinetics and Photochemical Data for Use in Atmospheric
719 Studies: Evaluation Number 18, Pasadena, CA, USA. [online] Available from:
720 <http://jpldataeval.jpl.nasa.gov/>, 2015.
- 721 Carlton, A. G., de Gouw, J., Jimenez, J. L., Ambrose, J. L., Attwood, A. R., Brown, S., Baker, K. R., Brock,
722 C., Cohen, R. C., Edgerton, S., Farkas, C. M., Farmer, D., Goldstein, A. H., Gratz, L., Guenther, A., Hunt, S.,
723 Jaeglé, L., Jaffe, D. A., Mak, J., McClure, C., Nenes, A., Nguyen, T. K., Pierce, J. R., de Sa, S., Selin, N. E.,
724 Shah, V., Shaw, S., Shepson, P. B., Song, S., Stutz, J., Surratt, J. D., Turpin, B. J., Warneke, C., Washenfelder,
725 R. A., Wennberg, P. O. and Zhou, X.: Synthesis of the Southeast Atmosphere Studies: Investigating
726 Fundamental Atmospheric Chemistry Questions, *Bull. Am. Meteorol. Soc.*, 99(3), 547–567,
727 doi:10.1175/BAMS-D-16-0048.1, 2018.
- 728 Carter, W. P. L., Cocker, D. R., Fitz, D. R., Malkina, I. L., Bumiller, K., Sauer, C. G., Pisano, J. T., Bufalino, C.
729 and Song, C.: A new environmental chamber for evaluation of gas-phase chemical mechanisms and
730 secondary aerosol formation, *Atmos. Environ.*, 39(40), 7768–7788,
731 doi:10.1016/j.atmosenv.2005.08.040, 2005.
- 732 Cocker, D. R., Flagan, R. C. and Seinfeld, J. H.: State-of-the-Art Chamber Facility for Studying Atmospheric
733 Aerosol Chemistry, *Environ. Sci. Technol.*, 35(12), 2594–2601, doi:10.1021/es0019169, 2001.
- 734 Crounse, J. D., Nielsen, L. B., Jørgensen, S., Kjaergaard, H. G. and Wennberg, P. O.: Autoxidation of
735 organic compounds in the atmosphere, *J. Phys. Chem. Lett.*, 4, 3513–3520, doi:10.1021/jz4019207,
736 2013.
- 737 D'Ambro, E. L., Møller, K. H., Lopez-Hilfiker, F. D., Schobesberger, S., Liu, J., Shilling, J. E., Lee, B. H.,
738 Kjaergaard, H. G. and Thornton, J. A.: Isomerization of Second-Generation Isoprene Peroxy Radicals:
739 Epoxide Formation and Implications for Secondary Organic Aerosol Yields, *Environ. Sci. Technol.*, 51(9),
740 4978–4987, doi:10.1021/acs.est.7b00460, 2017.
- 741 Fittschen, C., Whalley, L. K. and Heard, D. E.: The reaction of CH₃O₂ radicals with OH radicals: a
742 neglected sink for CH₃O₂ in the remote atmosphere., *Environ. Sci. Technol.*, 48(14), 7700–1,
743 doi:10.1021/es502481q, 2014.



- 744 Fry, J. L., Draper, D. C., Zarzana, K. J., Campuzano-Jost, P., Day, D. A., Jimenez, J. L., Brown, S. S., Cohen,
745 R. C., Kaser, L., Hansel, A., Cappellin, L., Karl, T., Hodzic Roux, A., Turnipseed, A., Cantrell, C., Lefer, B. L.
746 and Grossberg, N.: Observations of gas- and aerosol-phase organic nitrates at BEACHON-RoMBAS 2011,
747 Atmos. Chem. Phys., 13(17), 8585–8605, doi:10.5194/acp-13-8585-2013, 2013.
- 748 Hu, W., Palm, B. B., Day, D. A., Campuzano-Jost, P., Krechmer, J. E., Peng, Z., de Sá, S. S., Martin, S. T.,
749 Alexander, M. L., Baumann, K., Hacker, L., Kiendler-Scharr, A., Koss, A. R., de Gouw, J. A., Goldstein, A.
750 H., Seco, R., Sjostedt, S. J., Park, J.-H., Guenther, A. B., Kim, S., Canonaco, F., Prévôt, A. S. H., Brune, W.
751 H. and Jimenez, J. L.: Volatility and lifetime against OH heterogeneous reaction of ambient isoprene-
752 epoxydiols-derived secondary organic aerosol (IEPOX-SOA), Atmos. Chem. Phys., 16(18), 11563–11580,
753 doi:10.5194/acp-16-11563-2016, 2016.
- 754 Jørgensen, S., Knap, H. C., Otkjær, R. V., Jensen, A. M., Kjeldsen, M. L. H., Wennberg, P. O. and Kjaergaard,
755 H. G.: Rapid Hydrogen Shift Scrambling in Hydroperoxy-Substituted Organic Peroxy Radicals, J. Phys.
756 Chem. A, 120(2), 266–275, doi:10.1021/acs.jpca.5b06768, 2016.
- 757 Kalafut-Pettibone, A. J., Klems, J. P., Burgess, D. R. and McGivern, W. S.: Alkylperoxy radical
758 photochemistry in organic aerosol formation processes., J. Phys. Chem. A, 117(51), 14141–50,
759 doi:10.1021/jp4094996, 2013.
- 760 Kang, E., Root, M. J., Toohey, D. W. and Brune, W. H.: Introducing the concept of Potential Aerosol Mass
761 (PAM), Atmos. Chem. Phys., 7(22), 5727–5744, doi:10.5194/acp-7-5727-2007, 2007.
- 762 Kang, E., Toohey, D. W. and Brune, W. H.: Dependence of SOA oxidation on organic aerosol mass
763 concentration and OH exposure: experimental PAM chamber studies, Atmos. Chem. Phys., 11(4), 1837–
764 1852, doi:10.5194/acp-11-1837-2011, 2011.
- 765 Karjalainen, P., Timonen, H., Saukko, E., Kuuluvainen, H., Saarikoski, S., Aakko-Saksa, P., Murtonen, T.,
766 Bloss, M., Dal Maso, M., Simonen, P., Ahlberg, E., Svenningsson, B., Brune, W. H., Hillamo, R., Keskinen,
767 J. and Rönkkö, T.: Time-resolved characterization of primary particle emissions and secondary particle
768 formation from a modern gasoline passenger car, Atmos. Chem. Phys., 16(13), 8559–8570,
769 doi:10.5194/acp-16-8559-2016, 2016.
- 770 Klems, J. P., Lippa, K. a and McGivern, W. S.: Quantitative Evidence for Organic Peroxy Radical
771 Photochemistry at 254 nm, J. Phys. Chem. A, 119(2), 344–351, doi:10.1021/jp509165x, 2015.
- 772 Knap, H. C. and Jørgensen, S.: Rapid Hydrogen Shift Reactions in Acyl Peroxy Radicals, J. Phys. Chem. A,
773 121(7), 1470–1479, doi:10.1021/acs.jpca.6b12787, 2017.
- 774 Krechmer, J. E., Pagonis, D., Ziemann, P. J. and Jimenez, J. L.: Quantification of Gas-Wall Partitioning in
775 Teflon Environmental Chambers Using Rapid Bursts of Low-Volatility Oxidized Species Generated in Situ,
776 Environ. Sci. Technol., 50(11), 5757–5765, doi:10.1021/acs.est.6b00606, 2016.
- 777 Lambe, A., Massoli, P., Zhang, X., Canagaratna, M., Nowak, J., Daube, C., Yan, C., Nie, W., Onasch, T.,
778 Jayne, J., Kolb, C., Davidovits, P., Worsnop, D. and Brune, W.: Controlled nitric oxide production via
779 $O(\text{sup}\>1\text{<sup}\>D) + N\text{<sub}\>2\text{<sub}\>O$
780 reactions for use in oxidation flow reactor studies, Atmos. Meas. Tech., 10(6), 2283–2298,
781 doi:10.5194/amt-10-2283-2017, 2017.
- 782 Lambe, A. T. and Jimenez, J. L.: PAM Wiki: User Groups, [online] Available from:
783 <https://sites.google.com/site/pamwiki/user-groups> (Accessed 2 July 2018), 2018.
- 784 Lambe, A. T., Ahern, A. T., Williams, L. R., Slowik, J. G., Wong, J. P. S., Abbatt, J. P. D., Brune, W. H., Ng, N.
785 L., Wright, J. P., Croasdale, D. R., Worsnop, D. R., Davidovits, P. and Onasch, T. B.: Characterization of
786 aerosol photooxidation flow reactors: heterogeneous oxidation, secondary organic aerosol formation
787 and cloud condensation nuclei activity measurements, Atmos. Meas. Tech., 4(3), 445–461,
788 doi:10.5194/amt-4-445-2011, 2011.
- 789 Lambe, A. T., Cappa, C. D., Massoli, P., Onasch, T. B., Forestieri, S. D., Martin, A. T., Cummings, M. J.,
790 Croasdale, D. R., Brune, W. H., Worsnop, D. R. and Davidovits, P.: Relationship between Oxidation Level
791 and Optical Properties of Secondary Organic Aerosol, Environ. Sci. Technol., 47(12), 6349–6357,
792 doi:10.1021/es401043j, 2013.
- 793 Lambe, A. T., Chhabra, P. S., Onasch, T. B., Brune, W. H., Hunter, J. F., Kroll, J. H., Cummings, M. J., Brogan,
794 J. F., Parmar, Y., Worsnop, D. R., Kolb, C. E. and Davidovits, P.: Effect of oxidant concentration, exposure



- 795 time, and seed particles on secondary organic aerosol chemical composition and yield, *Atmos. Chem.*
796 *Phys.*, 15(6), 3063–3075, doi:10.5194/acp-15-3063-2015, 2015.
- 797 Levy II, H.: Normal atmosphere: large radical and formaldehyde concentrations predicted., *Science*,
798 173(3992), 141–143, doi:10.1126/science.173.3992.141, 1971.
- 799 Li, R., Palm, B. B., Ortega, A. M., Hu, W., Peng, Z., Day, D. A., Knote, C., Brune, W. H., de Gouw, J. and
800 Jimenez, J. L.: Modeling the radical chemistry in an Oxidation Flow Reactor (OFR): radical formation and
801 recycling, sensitivities, and OH exposure estimation equation, *J. Phys. Chem. A*, 119(19), 4418–4432,
802 doi:10.1021/jp509534k, 2015.
- 803 Lim, C. Y., Browne, E. C., Sugrue, R. A. and Kroll, J. H.: Rapid heterogeneous oxidation of organic coatings
804 on submicron aerosols, *Geophys. Res. Lett.*, 44(6), 2949–2957, doi:10.1002/2017GL072585, 2017.
- 805 Link, M. F., Friedman, B., Fulgham, R., Brophy, P., Galang, A., Jathar, S. H., Veres, P., Roberts, J. M. and
806 Farmer, D. K.: Photochemical processing of diesel fuel emissions as a large secondary source of isocyanic
807 acid (HNCO), *Geophys. Res. Lett.*, 43(8), 4033–4041, doi:10.1002/2016GL068207, 2016.
- 808 Mao, J., Ren, X., Brune, W. H., Olson, J. R., Crawford, J. H., Fried, a., Huey, L. G., Cohen, R. C., Heikes, B.,
809 Singh, H. B., Blake, D. R., Sachse, G. W., Diskin, G. S., Hall, S. R. and Shetter, R. E.: Airborne measurement
810 of OH reactivity during INTEX-B, *Atmos. Chem. Phys.*, 9(1), 163–173, doi:10.5194/acp-9-163-2009, 2009.
- 811 Martin, S. T., Artaxo, P., Machado, L. A. T., Manzi, A. O., Souza, R. A. F., Schumacher, C., Wang, J., Andreae,
812 M. O., Barbosa, H. M. J., Fan, J., Fisch, G., Goldstein, A. H., Guenther, A., Jimenez, J. L., Pöschl, U., Silva
813 Dias, M. A., Smith, J. N. and Wendisch, M.: Introduction: Observations and Modeling of the Green Ocean
814 Amazon (GoAmazon2014/5), *Atmos. Chem. Phys.*, 16(8), 4785–4797, doi:10.5194/acp-16-4785-2016,
815 2016.
- 816 Martin, S. T., Artaxo, P., Machado, L., Manzi, A. O., Souza, R. A. F., Schumacher, C., Wang, J., Biscaro, T.,
817 Brito, J., Calheiros, A., Jardine, K., Medeiros, A., Portela, B., De Sá, S. S., Adachi, K., Aiken, A. C., Alblbrecht,
818 R., Alexander, L., Andreae, M. O., Barbosa, H. M. J., Buseck, P., Chand, D., Comstomstock, J. M., Day,
819 D. A., Dubey, M., Fan, J., Fastst, J., Fisch, G., Fortner, E., Giangrande, S., Gillies, M., Goldstein, A. H.,
820 Guenther, A., Hubbbbe, J., Jensen, M., Jimenez, J. L., Keuttsch, F. N., Kim, S., Kuang, C., Laskskin, A.,
821 McKinney, K., Mei, F., Milller, M., Nascimento, R., Pauliquevis, T., Pekour, M., Peres, J., Petäjä, T.,
822 Pöhlkker, C., Pöschl, U., Rizzo, L., Schmid, B., Shillling, J. E., Silva Dias, M. A., Smith, J. N., Tomlinson,
823 J. M., Tóta, J. and Wendisch, M.: The green ocean amazon experiment (GOAMAZON2014/5) observes
824 pollution affecting gases, aerosols, clouds, and rainfall over the rain forest, *Bull. Am. Meteorol. Soc.*,
825 98(5), 981–997, doi:10.1175/BAMS-D-15-00221.1, 2017.
- 826 Matsunaga, A. and Ziemann, P. J.: Gas-Wall Partitioning of Organic Compounds in a Teflon Film Chamber
827 and Potential Effects on Reaction Product and Aerosol Yield Measurements, *Aerosol Sci. Technol.*, 44(10),
828 881–892, doi:10.1080/02786826.2010.501044, 2010.
- 829 Müller, J.-F., Liu, Z., Nguyen, V. S., Stavrakou, T., Harvey, J. N. and Peeters, J.: The reaction of methyl
830 peroxy and hydroxyl radicals as a major source of atmospheric methanol, *Nat. Commun.*, 7(May), 13213,
831 doi:10.1038/ncomms13213, 2016.
- 832 Nault, B. A., Campuzano-Jost, P., Day, D. A., Schroder, J. C., Anderson, B., Beyersdorf, A. J., Blake, D. R.,
833 Brune, W. H., Choi, Y., Corr, C. A., de Gouw, J. A., Dibb, J., DiGangi, J. P., Diskin, G. S., Fried, A., Huey, L.
834 G., Kim, M. J., Knote, C. J., Lamb, K. D., Lee, T., Park, T., Pusede, S. E., Scheuer, E., Thornhill, K. L., Woo,
835 J.-H. and Jimenez, J. L.: Secondary Organic Aerosol Production from Local Emissions Dominates the
836 Organic Aerosol Budget over Seoul, South Korea, during KORUS-AQ, *Atmos. Chem. Phys. Discuss.*, 1–69,
837 doi:10.5194/acp-2018-838, 2018.
- 838 Nel, A.: Air Pollution-Related Illness: Effects of Particles, *Science* (80-.), 308(5723), 804–806,
839 doi:10.1126/science.1108752, 2005.
- 840 Nguyen, T. B., Crounse, J. D., Schwantes, R. H., Teng, A. P., Bates, K. H., Zhang, X., St. Clair, J. M., Brune,
841 W. H., Tyndall, G. S., Keuttsch, F. N., Seinfeld, J. H. and Wennberg, P. O.: Overview of the Focused Isoprene
842 eXperiment at the California Institute of Technology (FIXCIT): mechanistic chamber studies on the
843 oxidation of biogenic compounds, *Atmos. Chem. Phys.*, 14(24), 13531–13549, doi:10.5194/acp-14-
844 13531-2014, 2014.
- 845 Orlando, J. J. and Tyndall, G. S.: Laboratory studies of organic peroxy radical chemistry: an overview with



- 846 emphasis on recent issues of atmospheric significance, *Chem. Soc. Rev.*, 41(19), 6294,
847 doi:10.1039/c2cs35166h, 2012.
- 848 Ortega, A. M., Day, D. A., Cubison, M. J., Brune, W. H., Bon, D., de Gouw, J. A. and Jimenez, J. L.:
849 Secondary organic aerosol formation and primary organic aerosol oxidation from biomass-burning
850 smoke in a flow reactor during FLAME-3, *Atmos. Chem. Phys.*, 13(22), 11551–11571, doi:10.5194/acp-
851 13-11551-2013, 2013.
- 852 Ortega, A. M., Hayes, P. L., Peng, Z., Palm, B. B., Hu, W., Day, D. A., Li, R., Cubison, M. J., Brune, W. H.,
853 Graus, M., Warneke, C., Gilman, J. B., Kuster, W. C., de Gouw, J., Gutiérrez-Montes, C. and Jimenez, J. L.:
854 Real-time measurements of secondary organic aerosol formation and aging from ambient air in an
855 oxidation flow reactor in the Los Angeles area, *Atmos. Chem. Phys.*, 16(11), 7411–7433,
856 doi:10.5194/acp-16-7411-2016, 2016.
- 857 Ortega, J., Turnipseed, A., Guenther, A. B., Karl, T. G., Day, D. A., Gochis, D., Huffman, J. A., Prenni, A. J.,
858 Levin, E. J. T., Kreidenweis, S. M., DeMott, P. J., Tobo, Y., Patton, E. G., Hodzic, A., Cui, Y. Y., Harley, P. C.,
859 Hornbrook, R. S., Apel, E. C., Monson, R. K., Eller, A. S. D., Greenberg, J. P., Barth, M. C., Campuzano-Jost,
860 P., Palm, B. B., Jimenez, J. L., Aiken, A. C., Dubey, M. K., Geron, C., Offenberg, J., Ryan, M. G., Fornwalt,
861 P. J., Pryor, S. C., Keutsch, F. N., Digangi, J. P., Chan, A. W. H., Goldstein, A. H., Wolfe, G. M., Kim, S., Kaser,
862 L., Schnitzhofer, R., Hansel, A., Cantrell, C. A., Mauldin, R. L. and Smith, J. N.: Overview of the Manitou
863 experimental forest observatory: Site description and selected science results from 2008 to 2013, *Atmos.*
864 *Chem. Phys.*, 14(12), 6345–6367, doi:10.5194/acp-14-6345-2014, 2014.
- 865 Palm, B. B., Campuzano-Jost, P., Ortega, A. M., Day, D. A., Kaser, L., Jud, W., Karl, T., Hansel, A., Hunter, J.
866 F., Cross, E. S., Kroll, J. H., Peng, Z., Brune, W. H. and Jimenez, J. L.: In situ secondary organic aerosol
867 formation from ambient pine forest air using an oxidation flow reactor, *Atmos. Chem. Phys.*, 16(5),
868 2943–2970, doi:10.5194/acp-16-2943-2016, 2016.
- 869 Palm, B. B., Campuzano-Jost, P., Day, D. A., Ortega, A. M., Fry, J. L., Brown, S. S., Zarzana, K. J., Dube, W.,
870 Wagner, N. L., Draper, D. C., Kaser, L., Jud, W., Karl, T., Hansel, A., Gutiérrez-Montes, C. and Jimenez, J.
871 L.: Secondary organic aerosol formation from in situ OH, O₃, and NO₃ oxidation of ambient forest air in
872 an oxidation flow reactor, *Atmos. Chem. Phys.*, 17(8), 5331–5354, doi:10.5194/acp-17-5331-2017, 2017.
- 873 Peng, Z. and Jimenez, J. L.: Modeling of the chemistry in oxidation flow reactors with high initial NO,
874 *Atmos. Chem. Phys.*, 17(19), 11991–12010, doi:10.5194/acp-17-11991-2017, 2017.
- 875 Peng, Z., Day, D. A., Stark, H., Li, R., Lee-Taylor, J., Palm, B. B., Brune, W. H. and Jimenez, J. L.: HO_x radical
876 chemistry in oxidation flow reactors with low-pressure mercury lamps systematically examined by
877 modeling, *Atmos. Meas. Tech.*, 8(11), 4863–4890, doi:10.5194/amt-8-4863-2015, 2015.
- 878 Peng, Z., Day, D. A., Ortega, A. M., Palm, B. B., Hu, W., Stark, H., Li, R., Tsigaridis, K., Brune, W. H. and
879 Jimenez, J. L.: Non-OH chemistry in oxidation flow reactors for the study of atmospheric chemistry
880 systematically examined by modeling, *Atmos. Chem. Phys.*, 16(7), 4283–4305, doi:10.5194/acp-16-
881 4283-2016, 2016.
- 882 Peng, Z., Palm, B. B., Day, D. A., Talukdar, R. K., Hu, W., Lambe, A. T., Brune, W. H. and Jimenez, J. L.:
883 Model Evaluation of New Techniques for Maintaining High-NO Conditions in Oxidation Flow Reactors
884 for the Study of OH-Initiated Atmospheric Chemistry, *ACS Earth Sp. Chem.*, 2(2), 72–86,
885 doi:10.1021/acsearthspacechem.7b00070, 2018.
- 886 Platt, S. M., El Haddad, I., Zardini, a. a., Clairrotte, M., Astorga, C., Wolf, R., Slowik, J. G., Temime-Roussel,
887 B., Marchand, N., Ježek, I., Drinovec, L., Močnik, G., Möhler, O., Richter, R., Barmet, P., Bianchi, F.,
888 Baltensperger, U. and Prévôt, a. S. H.: Secondary organic aerosol formation from gasoline vehicle
889 emissions in a new mobile environmental reaction chamber, *Atmos. Chem. Phys.*, 13(18), 9141–9158,
890 doi:10.5194/acp-13-9141-2013, 2013.
- 891 Praske, E., Otkjær, R. V., Crouse, J. D., Hethcox, J. C., Stoltz, B. M., Kjaergaard, H. G. and Wennberg, P.
892 O.: Atmospheric autoxidation is increasingly important in urban and suburban North America, *Proc. Natl.*
893 *Acad. Sci.*, 115(1), 64–69, doi:10.1073/pnas.1715540115, 2018.
- 894 Presto, A. A., Huff Hartz, K. E. and Donahue, N. M.: Secondary Organic Aerosol Production from Terpene
895 Ozonolysis. 1. Effect of UV Radiation, *Environ. Sci. Technol.*, 39(18), 7036–7045,
896 doi:10.1021/es050174m, 2005.

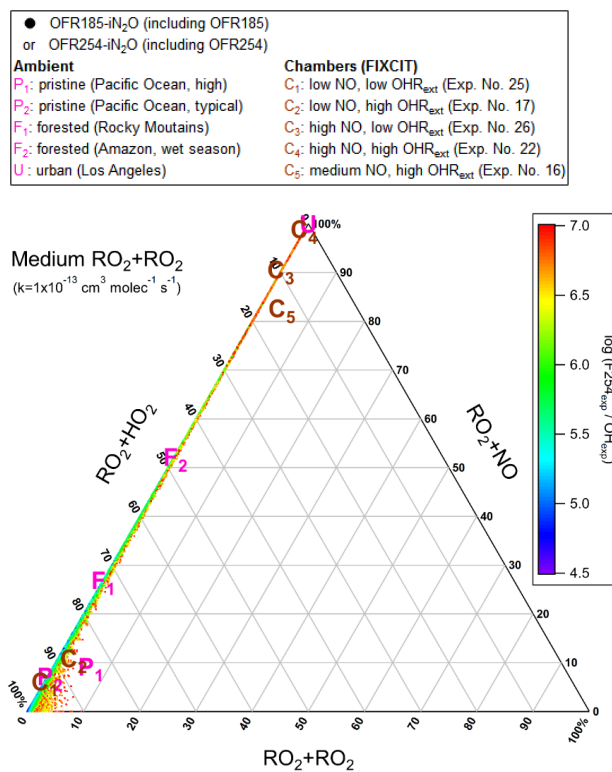


- 897 Richards-Henderson, N. K., Goldstein, A. H. and Wilson, K. R.: Large Enhancement in the Heterogeneous
898 Oxidation Rate of Organic Aerosols by Hydroxyl Radicals in the Presence of Nitric Oxide, *J. Phys. Chem.*
899 *Lett.*, 6, 4451–4455, doi:10.1021/acs.jpcclett.5b02121, 2015.
- 900 Richards-Henderson, N. K., Goldstein, A. H. and Wilson, K. R.: Sulfur Dioxide Accelerates the
901 Heterogeneous Oxidation Rate of Organic Aerosol by Hydroxyl Radicals, *Environ. Sci. Technol.*, 50(7),
902 3554–3561, doi:10.1021/acs.est.5b05369, 2016.
- 903 Ryerson, T. B., Andrews, A. E., Angevine, W. M., Bates, T. S., Brock, C. A., Cairns, B., Cohen, R. C., Cooper,
904 O. R., De Gouw, J. A., Fehsenfeld, F. C., Ferrare, R. A., Fischer, M. L., Flagan, R. C., Goldstein, A. H., Hair,
905 J. W., Hardesty, R. M., Hostetler, C. A., Jimenez, J. L., Langford, A. O., McCauley, E., McKeen, S. A., Molina,
906 L. T., Nenes, A., Oltmans, S. J., Parrish, D. D., Pederson, J. R., Pierce, R. B., Prather, K., Quinn, P. K., Seinfeld,
907 J. H., Senff, C. J., Sorooshian, A., Stutz, J., Surratt, J. D., Trainer, M., Volkamer, R., Williams, E. J. and Wofsy,
908 S. C.: The 2010 California Research at the Nexus of Air Quality and Climate Change (CalNex) field study,
909 *J. Geophys. Res. Atmos.*, 118(11), 5830–5866, doi:10.1002/jgrd.50331, 2013.
- 910 Stocker, T. F., Qin, D., Plattner, G.-K., Tignor, M., Allen, S. K., Boschung, J., Nauels, A., Xia, Y., Bex, V. and
911 Midgley, P. M.: *Climate Change 2013 - The Physical Science Basis*, edited by Intergovernmental Panel on
912 Climate Change, Cambridge University Press, Cambridge., 2014.
- 913 Stone, D., Whalley, L. K. and Heard, D. E.: Tropospheric OH and HO₂ radicals: field measurements and
914 model comparisons, *Chem. Soc. Rev.*, 41(19), 6348, doi:10.1039/c2cs35140d, 2012.
- 915 Tkacik, D. S., Lambe, A. T., Jathar, S., Li, X., Presto, A. A., Zhao, Y., Blake, D., Meinardi, S., Jayne, J. T.,
916 Croteau, P. L. and Robinson, A. L.: Secondary Organic Aerosol Formation from in-Use Motor Vehicle
917 Emissions Using a Potential Aerosol Mass Reactor, *Environ. Sci. Technol.*, 48(19), 11235–11242,
918 doi:10.1021/es502239v, 2014.
- 919 Wang, J., Doussin, J. F., Perrier, S., Perraudin, E., Katrib, Y., Pangui, E. and Picquet-Varrault, B.: Design of
920 a new multi-phase experimental simulation chamber for atmospheric photochemistry, aerosol and cloud
921 chemistry research, *Atmos. Meas. Tech.*, 4(11), 2465–2494, doi:10.5194/amt-4-2465-2011, 2011.
- 922 Wofsy, S. C., Apel, E., Blake, D. R., Brock, C. A., Brune, W. H., Bui, T. P., Daube, B. C., Dibb, J. E., Diskin, G.
923 S., Elkiins, J. W., Froyd, K., Hall, S. R., Hanisco, T. F., Huey, L. G., Jimenez, J. L., McKain, K., Montzka, S. A.,
924 Ryerson, T. B., Schwarz, J. P., Stephens, B. B., Weinzierl, B. and Wennberg, P.: *ATOM: Merged Atmospheric
925 Chemistry, Trace Gases, and Aerosols*, Oak Ridge, Tennessee, USA., 2018.
- 926 Yan, C., Kocevskaja, S. and Krasnoperov, L. N.: Kinetics of the Reaction of CH₃O₂ Radicals with OH Studied
927 over the 292–526 K Temperature Range, *J. Phys. Chem. A*, 120(31), 6111–6121,
928 doi:10.1021/acs.jpca.6b04213, 2016.
- 929 Zhang, X., Cappa, C. D., Jathar, S. H., McVay, R. C., Ensberg, J. J., Kleeman, M. J. and Seinfeld, J. H.:
930 Influence of vapor wall loss in laboratory chambers on yields of secondary organic aerosol., *Proc. Natl.*
931 *Acad. Sci. U. S. A.*, 111(16), 5802–7, doi:10.1073/pnas.1404727111, 2014.
- 932 Ziemann, P. J. and Atkinson, R.: Kinetics, products, and mechanisms of secondary organic aerosol
933 formation, *Chem. Soc. Rev.*, 41(19), 6582, doi:10.1039/c2cs35122f, 2012.

934



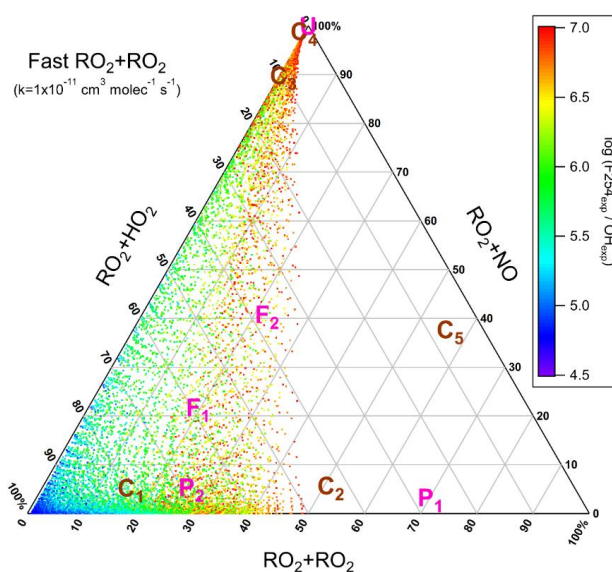
935



936

937

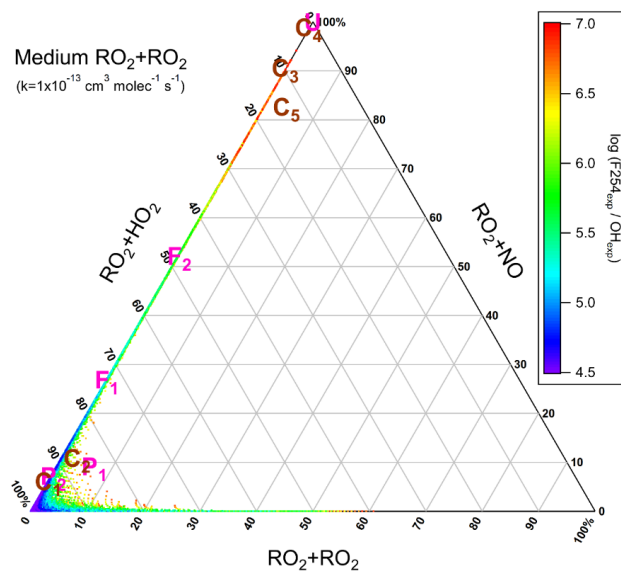
(a) OFR185



938

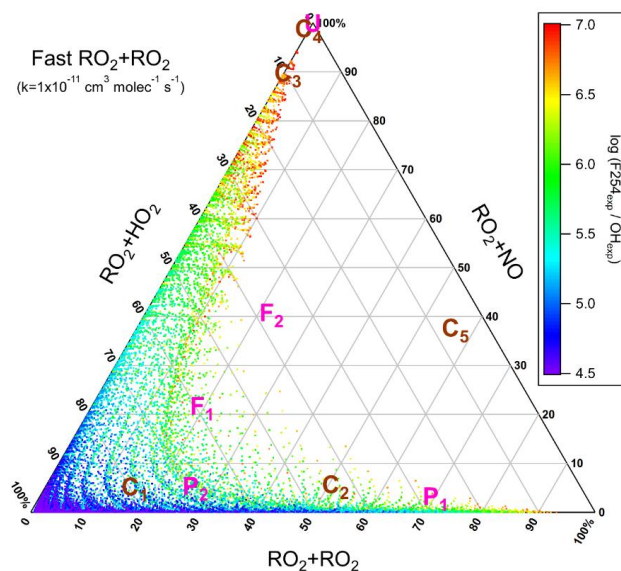
939

(b) OFR185



(c) OFR254-70

941



(d) OFR254-70

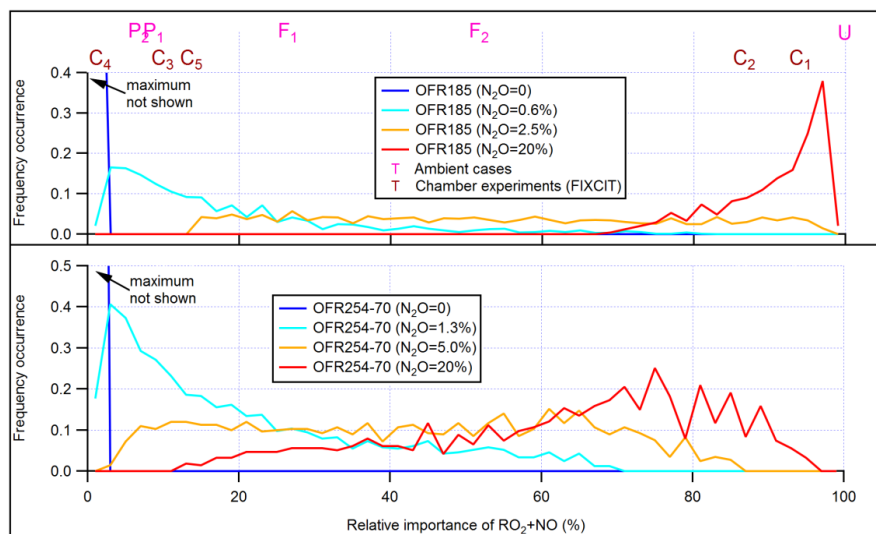
943

944 **Figure 1.** Triangle plots of RO_2 fate by RO_2+HO_2 , RO_2+RO_2 and RO_2+NO (without RO_2+OH and RO_2
 945 isomerization considered in the model) for RO_2 with the medium self/cross reaction rate constant (1×10^{-13}
 946 $\text{cm}^3 \text{ molec}^{-1} \text{ s}^{-1}$) in (a) OFR185 (including OFR185- iN_2O) and (c) OFR254-70 (including OFR254-70-
 947 iN_2O) and for RO_2 with the fast self/cross reaction rate constant ($1 \times 10^{-11} \text{ cm}^3 \text{ molec}^{-1} \text{ s}^{-1}$) in (b)
 948 OFR185 (including OFR185- iN_2O) and (d) OFR254-70 (including OFR254-70- iN_2O). Inclined tick values on
 949 an axis indicate the grid lines that should be followed (in parallel to the inclination) to read the



950 corresponding values on this axis. The OFR data points are colored by the logarithm of the exposure ratio
951 between 254 nm photon flux and OH, a measure of badness of OFR conditions in terms of 254 nm organic
952 photolysis. Several typical ambient and chamber cases (see Table 2 for details of these cases) are also
953 shown for comparison.

954



955

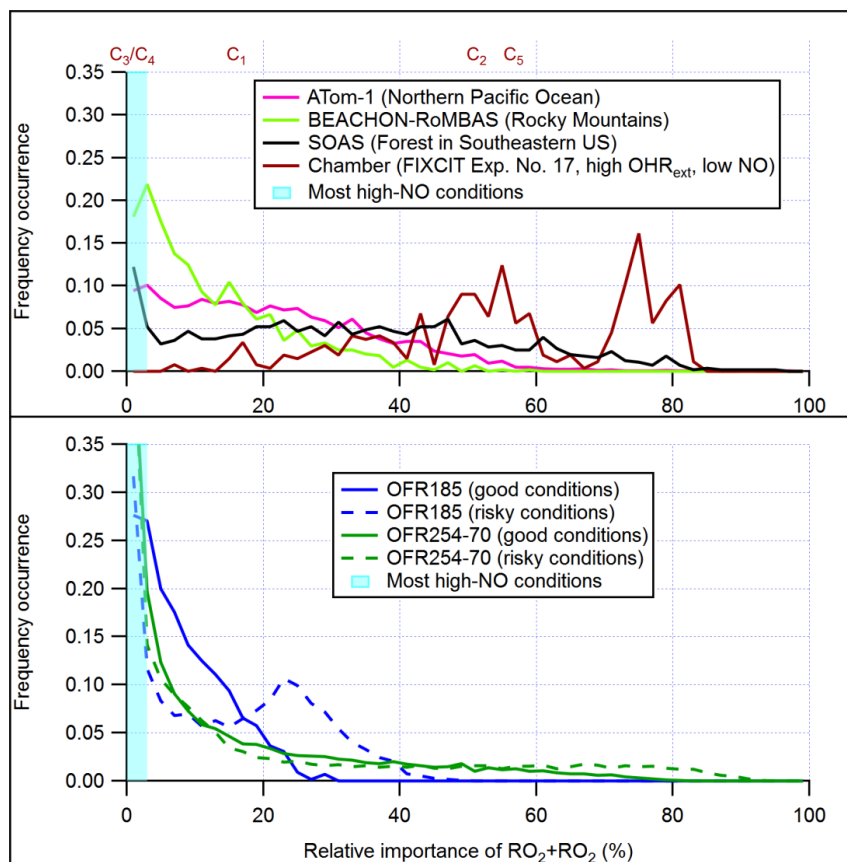
956

Figure 2. Frequency distributions of the relative importance of RO_2+NO in the fate of RO_2 (with medium self/cross reaction rate constant and without RO_2+OH and RO_2 isomerization considered) for OFR185 (including OFR185- $i\text{N}_2\text{O}$) and OFR254-70 (including OFR254-70- $i\text{N}_2\text{O}$). Distributions for several different N_2O levels are shown. Only good and risky conditions (in terms of non-tropospheric organic photolysis) are included in the distributions. Also shown is the relative importance of RO_2+NO for several typical ambient and chamber cases (see Table 2 for details of these cases).

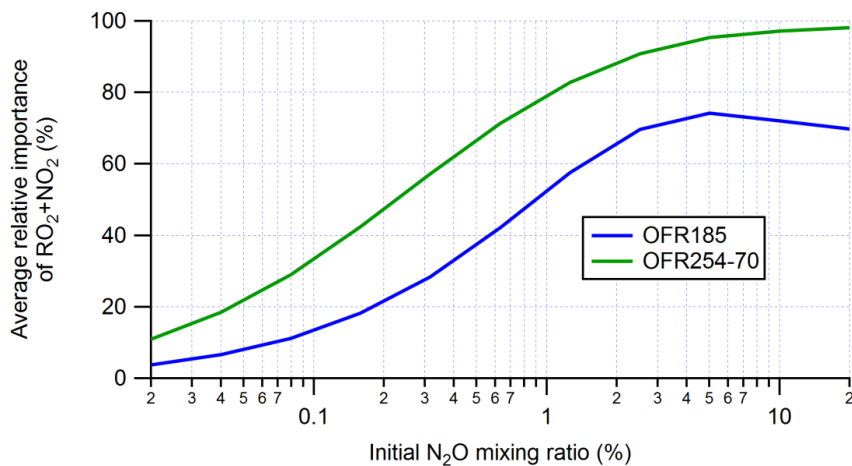
960

961

962



963
 964 **Figure 3.** Frequency distributions of the relative importance of RO_2+RO_2 in the fate of RO_2 (with fast
 965 self/cross reaction rate constant and without RO_2+OH and RO_2 isomerization considered) for OFR185
 966 (including OFR185- iN_2O), OFR254-70 (including OFR254-70- iN_2O) and a chamber experiment and in the
 967 atmosphere (a couple of different environments). The OFR distributions for good and risky conditions (in
 968 terms of 254 nm organic photolysis, see Table S1 for the definitions of these conditions) are shown
 969 separately. Also shown is the relative importance of RO_2+RO_2 for several typical chamber cases (see Table
 970 2 for details of these cases). The range of the RO_2+RO_2 relative importance for most high-NO
 971 conditions is highlighted in cyan.
 972



973

974

975

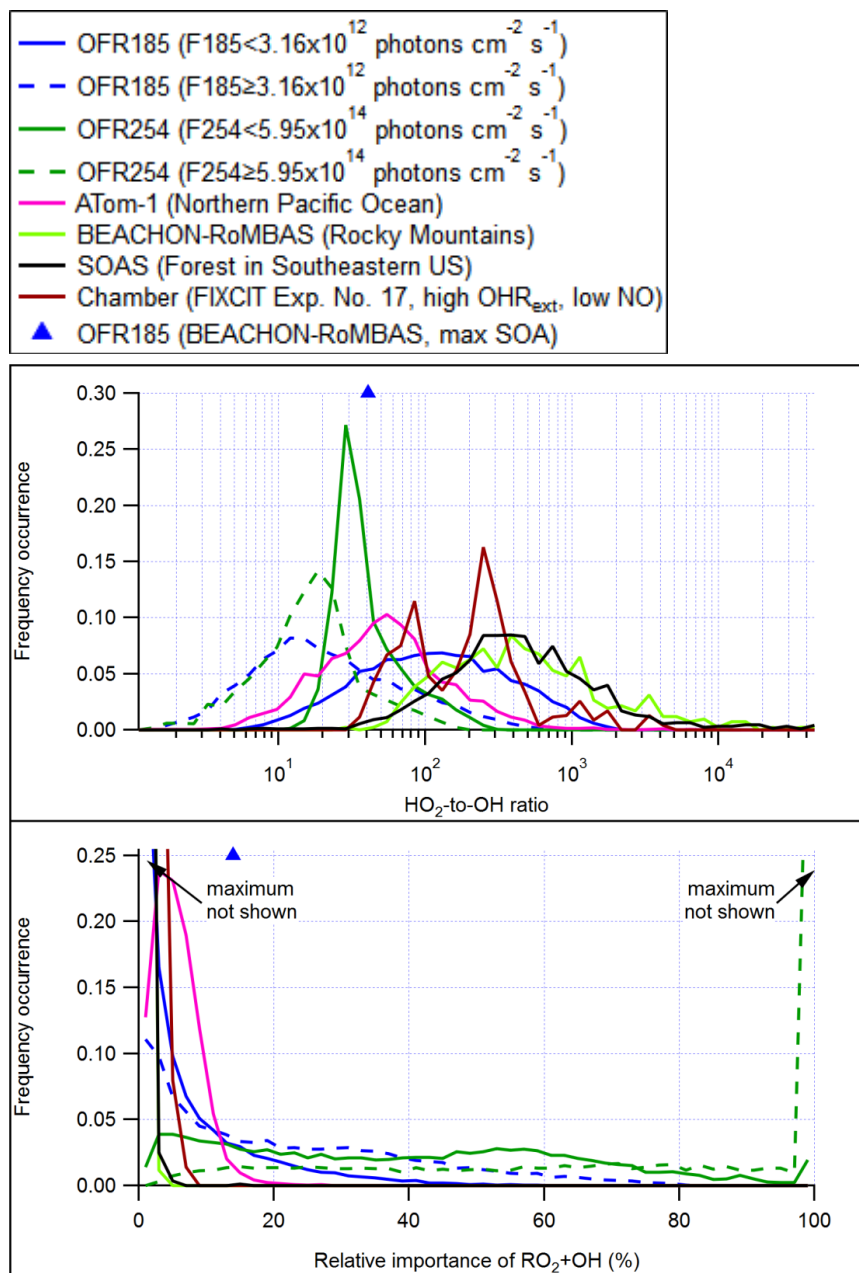
976

977

Figure 4. Average relative importance of RO₂+NO₂ in acyl RO₂ fate (RO₂+OH and RO₂ isomerization not considered) in OFR185 (including OFR185-iN₂O) and OFR254-70 (including OFR254-70-iN₂O). The averages are calculated based on good and risky conditions (in terms of non-tropospheric organic photolysis) only.

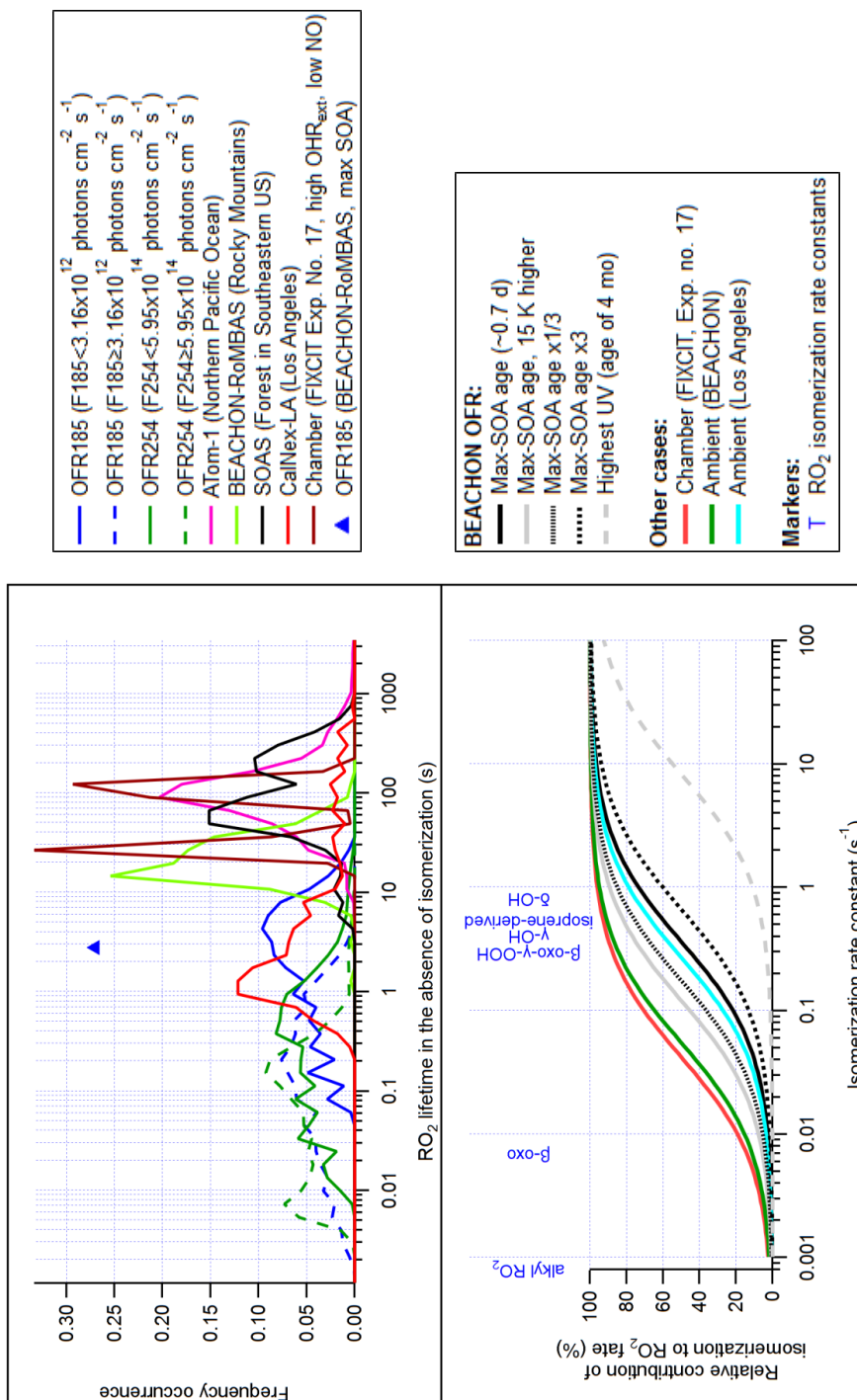


978



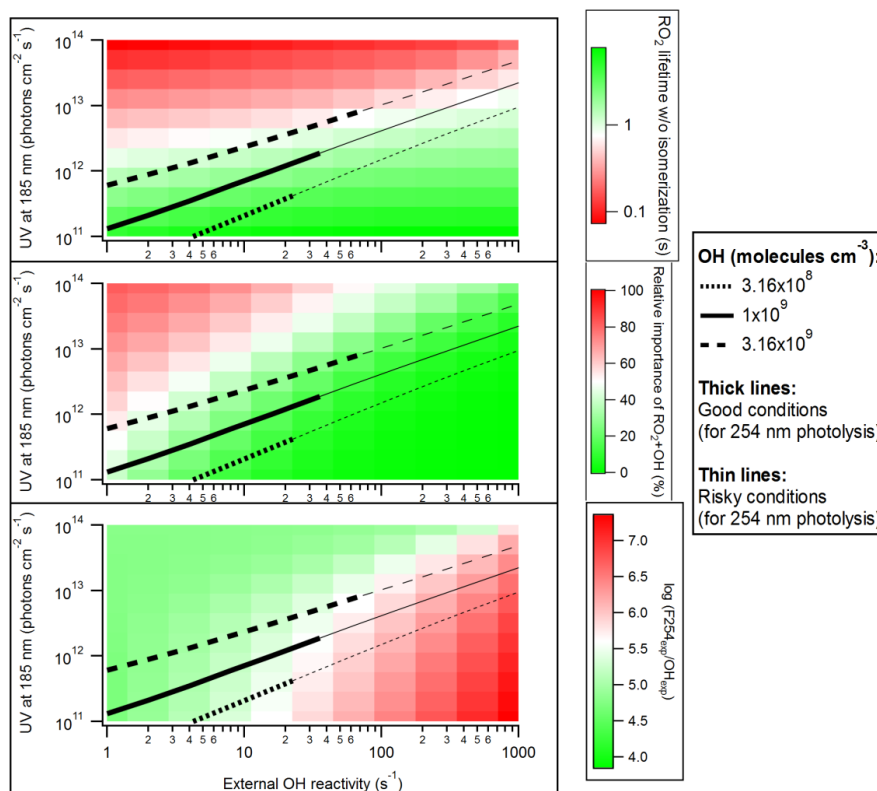
979

980 **Figure 5.** Frequency distributions of (top) the HO₂-to-OH ratio and (bottom) the relative importance of
 981 RO₂+OH in the fate of RO₂ (with medium self/cross reaction rate constant) for OFR185 (including OFR185-
 982 iN₂O), OFR254-70 (including OFR254-70-iN₂O) and a chamber experiment and in the atmosphere (a
 983 couple of different environments). The OFR distributions for lower (F185<3.16x10¹² photons cm⁻² s⁻¹;
 984 F254<5.95x10¹⁴ photons cm⁻² s⁻¹) and higher UV (F185≥3.16x10¹² photons cm⁻² s⁻¹; F254≥5.95x10¹⁴
 985 photons cm⁻² s⁻¹) are shown separately. Only good and risky conditions (in terms of non-tropospheric
 986 organic photolysis) are included in the distributions for OFRs. Also shown are the HO₂-to-OH and the
 987 relative importance of RO₂+OH for OFR experiments with ambient air input in field studies.





988 **Figure 6.** (top) Same format as Fig. 5, but for RO₂ lifetime (RO₂ isomerization included in the model but excluded from lifetime calculation). (bottom) Relative contribution of
989 isomerization to RO₂ fate as a function of RO₂ isomerization rate constant in several model cases for OFR experiments in the BEACHON-RoMIBAS campaign (Palm et al., 2016),
990 in a chamber experiment and in two ambient cases. Isomerization rate constants of several RO₂ (Crouse et al., 2013; Praske et al., 2018) are also shown.
991



992
993 **Figure 7.** (top) RO₂ lifetime in the absence of isomerization, (middle) relative importance of RO₂+OH in
994 RO₂ fate and (bottom) logarithm of the exposure ratio between 254 nm photon flux and OH as a function
995 of 185 nm photon flux and external OH reactivity for OFR185 at N₂O=0 and H₂O=2.3%. Three lines
996 denoting conditions leading to OH of 3.16 × 10⁸, 1 × 10⁹ and 3.16 × 10⁹ molecules cm⁻³, respectively, are
997 added in each panel. The thick and thin parts of these lines correspond to good and risky conditions (in
998 terms of 254 nm organic photolysis (which is usually worse than 185 nm organic photolysis; Peng et al.,
999 2016) respectively.
1000



1001 **Table 1.** Rate constants [in $\text{cm}^3 \text{ molecule}^{-1} \text{ s}^{-1}$ except for isomerization (in s^{-1})] / cross section (in cm^2) and
 1002 product(s) of RO_2 loss pathways. Only organic species are listed for product(s).

RO_2 loss pathway	Rate constant / cross section	Product(s)
$\text{RO}_2 + \text{HO}_2$	$1.5 \times 10^{-11} \text{ a}$	mainly ROOH for most RO_2 ^a
$\text{RO}_2 + \text{NO}$	$9 \times 10^{-12} \text{ a}$	RO, RONO_2 ^b
$\text{RO}_2 + \text{RO}_2$	Primary: $\sim 10^{-13} \text{ a}$ Secondary: $\sim 10^{-15} \text{ a}$ Tertiary: $\sim 10^{-17} \text{ a}$ Substituted: can be up to 2 orders of magnitude higher ^b Acyl: $\sim 10^{-11} \text{ b}$	ROH+R(=O), RO+RO, ROOR ^a
$\text{RO}_2 + \text{NO}_2$ (in OFRs)	$7 \times 10^{-12} \text{ c}$	RO_2NO_2 ^b
$\text{RO}_2 + \text{OH}$	$1 \times 10^{-10} \text{ d}$	ROOOH (for $\geq \text{C}_4 \text{ RO}_2$), RO (smaller RO_2) ^e
RO_2 isomerization	Autoxidation: $\sim 10^{-3} - 10^2 \text{ f}$ Other: up to 10^6 g	generally another RO_2
RO_2 photolysis	$\sim 10^{-18}$ at 254 nm ^h $\sim 10^{-21} - 10^{-19}$ in UVA and UVB ^h	mainly R, other photochemical products possible ⁱ
$\text{RO}_2 + \text{NO}_3$	$\sim 1 - 3 \times 10^{-12} \text{ b}$	RO^{b}
$\text{RO}_2 + \text{O}_3$	$\sim 10^{-17} \text{ b}$	RO^{b}

1003 ^a: Ziemann and Atkinson (2012);

1004 ^b: Orlando and Tyndall (2012);

1005 ^c: typical value within the reported range in Orlando and Tyndall (2012); thermal decomposition rate
 1006 constants of nitrates of acyl and non-acyl RO_2 are assumed to be 0.0004 and 3 s^{-1} , respectively, also
 1007 typical values within the reported ranges in Orlando and Tyndall (2012);

1008 ^d: value used in the present work based on Bossolasco et al. (2014); Assaf et al. (2016, 2017a); Müller
 1009 et al. (2016); Yan et al. (2016);

1010 ^e: Müller et al. (2016); Yan et al. (2016); Assaf et al. (2017b, 2018);

1011 ^f: Crouse et al. (2013);

1012 ^g: Knap and Jørgensen (2017);

1013 ^h: Burkholder et al. (2015);

1014 ⁱ: Klems et al. (2015).

1015



Table 2. Several typical ambient and chamber (the FIXCIT campaign) cases that are compared to OFR cases.

Type	Label	Case	OHR _{voc} (s ⁻¹)	OH	NO	HO ₂
Ambient	P ₁	Pristine (Pacific Ocean, high RO ₂) ^a	1.9	0.39 ppt	1.9 ppt	11 ppt
	P ₂	Pristine (Pacific Ocean, typical) ^a	1	0.25 ppt	3 ppt	25 ppt
	F ₁	Forested (Rocky Mountains) ^b	N/A ^c	1 ppt	60 ppt	100 ppt
	F ₂	Forested (Amazon, wet season) ^d	9.6	1.2x10 ⁶ molecules cm ⁻³	37 ppt	5.1x10 ⁸ molecules cm ⁻³
	U	Urban (Los Angeles) ^e	25 ^f	1.5x10 ⁶ molecules cm ^{-3g}	1.5 ppb ⁱ	1.5x10 ⁸ molecules cm ^{-3g}
Chamber (FIXCIT)	C ₁	Exp. No. 25 ^h	30.5 ⁱ	3x10 ⁶ molecules cm ⁻³	15 ppt	150 ppt
	C ₂	Exp. No. 17 ^h	116 ⁱ	1.2x10 ⁶ molecules cm ⁻³	10 ppt	50 ppt
	C ₃	Exp. No. 26 ^h	32 ⁱ	2x10 ⁷ molecules cm ⁻³	3.5 ppb	230 ppt
	C ₄	Exp. No. 22 ^h	147 ⁱ	2.3x10 ⁶ molecules cm ⁻³	430 ppb	4.3 ppb
	C ₅	Exp. No. 16 ^h	45.7 ⁱ	4x10 ⁶ molecules cm ⁻³	80 ppt	8 ppt

^a: Wofsy et al. (2018) for the Atom-1 Campaign;

^b: Fry et al. (2013), for the BEACHON-RoMBAS campaign;

^c: RO₂ concentration was given in Fry et al. (2013) (50 ppt), so that OHR_{voc} is not needed for RO₂ fate estimation;

^d: personal communication from Daun Jeong and Saewung Kim for the GoAmazon Campaign (Martin et al., 2016, 2017);

^e: typical case in the CalNex-LA campaign (Ryerson et al., 2013);

^f: estimated (Peng et al., 2016);

^g: typical ambient value (Mao et al., 2009; Stone et al., 2012);

^h: data from Nguyen et al. (2014);

ⁱ: initial value.

1016

1017

1018

1019

1020

1021

1022

1023

1024

1025

1026